AALTO UNIVERSITY
School of Science
Department of Applied Physics

Jani Mikkola

Modelling of smart multi-energy carrier networks for sustainable cities

Master's Thesis submitted in partial fulfillment of the requirements for the degree of Master of Science in Technology in the Degree Programme in Engineering Physics and Mathematics.

Espoo, January 9, 2012

Supervisor: Professor Peter Lund
Instructor: M.Sc. Rami Niemi

AALTO UNIVERSITY
SCHOOL OF SCIENCE

ABSTRACT OF THE
MASTER'S THESIS

Author:	Jani Mikkola		
Title:	Modelling of smart multi-energy carrier networks for sustainable cities		
Title in Finnish:	Älykkäiden monienergiaverkkojen mallinnus kestävissä kaupunkiympäristöissä		
Degree Programme:	Degree Programme in Engineering Physics and Mathematics		
Major Subject:	Advanced Energy Systems	**Minor Subject:**	Systems Sciences
Chair (code):	Tfy-56		
Supervisor:	Prof. Peter Lund	**Instructor:**	M.Sc. Rami Niemi

Abstract:

Multi-energy carrier networks constitute a concept where several energy carriers are considered simultaneously, for example electrical, natural gas and district heating networks. In this thesis, a spatial and temporal model for multi-energy carrier studies based on MATLAB® is represented. In the model, a city is divided into interconnected nodes with different energy networks. Each node has its own production and consumption profile. At each node it is possible to convert energy to another type of energy, store it, or transfer it to the networks.

The model was used to analyze the impacts of large-scale renewable energy penetration in present energy systems. An important research question was how much more renewable energy capacity and system flexibility can be achieved with a multi-energy approach. Helsinki and Shanghai were chosen as the cases for urban areas.

In Helsinki, the focus was on a large offshore wind farm and solar energy utilization together with smart electric vehicle charging. It was found that the wind power capacity in Helsinki could be increased by more than three times from the reference case with an electricity-to-heat conversion scheme. It was also shown that a smart and predictive recharging strategy for electric vehicles may solve the problems associated with high and intermittent solar production when it overstresses the electrical network.

In the densely populated Shanghai, the solar electricity could momentarily satisfy the whole electricity demand on an hourly basis. On a yearly scale, 20 % of the electricity and 18 % of all energy could be from solar production. These shares of distributed energy production could be raised to over 30 % with fuel cell based trigeneration system in the city center without still exceeding the self-consumption limit.

Date:	Jan 9, 2012	**Language:**	English	**Number of pages:**	70

Keywords: Multi-energy carrier network, smart grid, renewable energy, modelling

AALTO-YLIOPISTO
PERUSTIETEIDEN KORKEAKOULU DIPLOMITYÖN TIIVISTELMÄ

Tekijä:	Jani Mikkola		
Työn nimi:	Älykkäiden monienergiaverkkojen mallinnus kestävissä kaupunkiympäristöissä		
Title in English:	Modelling of smart multi-energy carrier networks for sustainable cities		
Tutkinto-ohjelma:	Teknillisen fysiikan ja matematiikan tutkinto-ohjelma		
Pääaine:	Energiatieteet	**Sivuaine:**	Systeemitieteet
Opetusyksikön (ent. professuuri) koodi:	Tfy-56		
Työn valvoja:	Prof. Peter Lund	**Työn ohjaaja:**	FM Rami Niemi

Tiivistelmä:

Monienergiaverkot muodostavat konseptin, jossa monia eri energiasiirtotapoja, esimerkiksi sähkö-, maakaasu- ja kaukolämpöverkkoa, tutkitaan samanaikaisesti yhtenä kokonaisuutena. Tässä diplomityössä esitellään spatiaalinen ja ajallinen, MATLAB®:iin pohjautuva monienergiaverkkomalli. Mallissa kaupunki jaetaan noodeihin, jotka yhdistetään toisiinsa eri energiaverkoilla ja joilla on omat tuotanto- ja kulutusprofiilinsa. Noodeissa on mahdollista muuntaa energiaa muodosta toiseen, varastoida sitä, siirtää sitä verkkoihin tai käyttää sitä sieltä.
Mallia käytettiin analysoimaan laajamittaisen uusiutuvan energian hyödyntämisen vaikutuksia nykyiseen energiajärjestelmään. Pyrittiin selvittämään, paljonko lisää joustavuutta ja uusiutuvan energian kapasiteettia voidaan energiajärjestelmään monienergiatarkastelulla saavuttaa. Helsinki ja Shanghai valittiin tarkasteltaviksi kaupunkiympäristöiksi.
Helsingissä keskityttiin suureen merituulipuistoon ja aurinkovoimaan yhdistettynä sähköautojen lataamiseen. Saatiin selville, että Helsingin energiajärjestelmän tuulivoimakapasiteetti voitaisiin yli kolminkertaistaa muuntamalla sähköä kaukolämmöksi. Lisäksi osoitettiin, että älykkäällä sähköautojen latausstrategialla voidaan ratkoa ongelmia, joissa voimakas aurinkosähkötuotanto rasittaa sähköverkkoa liiaksi.
Tiivisti asutetussa Shanghaissa energiajärjestelmään mahtuisi aurinkovoimaa niin paljon, että hetkellisesti koko sähköntarve voitaisiin tyydyttää sillä. Vuositasolla tämä tarkoittaisi, että 20 % sähkön- ja 18 % koko energiantarpeesta tuotettaisiin aurinkovoimalla. Jos keskusta-alueelle asennetaan polttokennopohjaista sähkön, lämmön ja kylmän yhteistuotantoa, nämä hajautetun energiantuotannon osuudet voitaisiin nostaa yli 30 %:iin, silti viemättä energiaa lainkaan tuotantopiikkien aikana kaupungin ulkopuolelle.

Päivämäärä:	9.1.2012	**Kieli:**	Englanti	**Sivumäärä:**	70
Avainsanat:	Monienergiaverkot, älykäs sähköverkko, uusiutuva energia, mallinnus				

Acknowledgements

This Master's thesis has been done at the Department of Applied Physics at Aalto University School of Science. The work is part of SIMBe project (Smart Infrastructure for Electric Mobility in Built Environment) that was funded by Tekes (the Finnish Funding Agency for Technology and Innovation). The financial support is greatly appreciated.

I want to thank professor Peter Lund who has offered the possibility to be part of the scientific community and supported me throughout the work. At the same time I wish to express my thanks to everyone in the New Energy Technologies group, especially my room mates Rami Niemi and Juuso Lindgren. They are fantastic fellow workers that made the atmosphere at work inspiring and relaxing.

I would also like to thank all my fellow students and good friends in Otaniemi and at Aalto University. Their help with exercises and assignments during the studies as well as all the great and funny moments at free time have made my life in Helsinki and Espoo much easier and richer. These days will stay in my memory all my life.

Finally, my greatest gratitude goes to my parents and family. They have always been there for me and offered their absolute support and encouragement throughout my whole life. Words are not enough to describe how deeply I appreciate everything they have done for me.

Lopuksi suurimmat kiitokset kuuluvat vanhemmilleni ja perheelleni. He ovat olleet aina tukenani ja tarjonneet tinkimättömän apunsa ja kannustuksensa koko elämäni varrella, hyvinä ja huonoina hetkinä. Sanat eivät riitä kuvaamaan kuinka syvästi arvostan kaikkea, mitä he ovat vuokseni tehneet.

Otaniemi, January 9, 2012

Jani Mikkola

Contents

Nomenclature

Abbreviations

BIPV	Building-integrated Photovoltaics
CHP	Combined Heat and Power
CHCP	Combined Heat, Cooling and Power
COP	Coefficient Of Performance
DEGS	Distributed Energy Generation System
EV	Electric Vehicle
PHEV	Plug-in Hybrid Electric Vehicle
PV	Photovoltaics, Photovoltaic cell
SOFC	Solid Oxide Fuel Cell

Symbols

A	Area of the node (km^2)
A_p	Surface area of the pipe (m^2)
C	Energy conversion (MW)
D	Energy to be distributed outside the node (i.e. energy balance) (MW)
$\mathbf{D}$	Energy balance as a 2-element vector (MW)
d_i	Density of energy consumer type i (persons/km^2 *or* MW/km^2)
$d_{0,i}$	Maximum density of energy consumer type i (persons/km^2 *or* MW/km^2)
F	Energy flow in the lines of a network (MW)
$\mathbf{F}$	Energy flow as a 2-element vector (MW)
$\hat{F}$	Overflow (MW)
F_0	Heat flow after which the heat network temperature is being increased (MW)
$f^{(n)}$	Part of the flow that is produced at node n (MW)
$f^{(-n)}$	Part of the flow that is produced somewhere else than at node n (MW)

G	Outgoing energy flow (MW)
$\mathbf{G}$	Outgoing energy flow as a 2-element vector (MW)
h_i	Temporal base consumption profile of the consumer type i (MW/person *or none*)
I	Electric current (A)
k	Scaling factor of the heat/cooling losses ($\mathrm{MW}^{3/4}$)
L	Flow losses (MW)
$\tilde{L}_h$	Minimum heat loss at every time step (MW)
l	Line of the network
N	Net production (MW)
$\mathcal{N}$	Number of nodes
n	Node
P	Energy production (MW)
p	Pressure (Pa)
Q	Energy consumption (MW)
q_i	Total consumption profile of the consumer type i (MW)
$q^{(n)}$	Part of the consumed energy that is produced at node n (MW)
$q^{(-n)}$	Part of the consumption that is produced somewhere else than at node n (MW)
R	Resistance (Ω)
$\mathbf{r}$	Coordinate vector (km)
r_0	Distance that the consumer density is peaked at (km)
S	Stored energy (MWh)
$S_{\max}$	Maximum amount of energy that fits into the store (MWh)
s	Pipe length (km)
t	Time, time step (h)
U	Voltage (V)
W	Wasted energy, losses (MWh)
x_{in}	Share of free storage capacity that can be utilized at one time step
x_{out}	Share of stored energy that can be utilized at one time step
$\mathbf{Y}$	Matrix of the origins and destinations of energy (MW)
$\mathbf{y}_n$	Vector telling where does the energy produced at node n flow to (MW)
α	Width parameter of the density function ($1/\mathrm{km}^2$)
$\eta_{a\triangleright b}$	Conversion efficiency/COP from energy type a into energy type b
κ	Electrical loss coefficient in network cables (Ω/V^2, 1/MW)
λ	Heat loss coefficient in network pipes
ν	Kinematic viscosity (m^2/s)
ρ	Pipe radius (m)
ς	Efficiency for keeping energy in stores

ς_+ Efficiency for charging the stores

ς_- Efficiency for discharging the stores

Φ Flow channel (MW)

φ Mass flow rate (kg/s)

List of Figures

List of Tables

Chapter 1

Introduction

Since the early dawn of mankind, people have been more or less dependent on energy. The heat and light from the sun has made the human life and development possible. During the history until the second half of the 18th century, all energy usage was renewable. People learned how to make fire (burn wood), how to use wind power to sail or run wind mills or how to use water power.

However, this was about to change radically. New inventions, like Watt's steam engine, made the industrial revolution possible and the revolution brought wide-scale coal and oil exploitation with it. Since then the total energy demand has been growing exponentially and most of it has been satisfied with fossil fuels. The development has been continuing and still today fossil energy is by far the most important energy source.

Present energy use has caused adverse environmental impacts, e.g. emissions from fossil energy and nuclear power accidents. A true energy revolution may be necessary based on renewable and clean energy. The change, however, is not simple and the existing energy infrastructure puts its own requirements also to the new energy production.

The challenges and impacts of large-scale renewable energy exploitation are the main topics considered in this Master's thesis. There are two main issues that need consideration. First, energy production is about to change from large centralized power plants to more distributed local-scale production. This would bring a lot of small solar, biomass and wind power production plants all around. The energy networks, especially the electric grid, may be put to under stress in such a case. Another issue is the variability and intermittency of the new energy production. For example, wind speed varies over time and the sun shine is highly variable as well. A major challenge will be to compensate for the large variability.

Much of the discussion around energy is focused on electricity. Terms like power station and power grid are normally interpreted as explicitly referring to electricity production plant and electric network. This thesis tries to broaden the view of energy and its transportation

to other forms of final energy as well. In this thesis different types of energy networks in a city are examined. In addition to an electrical network, a district heating and cooling network and a natural gas line could be possible. These networks have considerable capacity to transport energy. An interesting question is to examine how such existing multi-energy networks and their cross-use could ease the problems around renewable energy intermittency.

The first part of the thesis represents the MATLAB® program that was created to model the multi-energy carrier networks and the energy consumption and production in the cities. The basic structure of the model, as well as the calculation principles for energy balances and energy transportation, are represented. In the second part, the model is used to simulate a couple of real world cases. The first case is Helsinki, a medium-sized northern city. The second one is Shanghai, a southern megacity. The energy systems of these cities are described and penetration schemes of renewable and sustainable energy technologies are analyzed. In Helsinki, the main focus is on wind power and solar electricity combined with electric vehicles, and in Shanghai on solar energy and local small-scale trigeneration.

This work was done at Aalto University, Department of Applied Physics in the New Energy Technologies Group. The funding came from Tekes (the Finnish Funding Agency for Technology and Innovation) through the SIMBe project (Smart Infrastructure for Electric Mobility in Built Environment).

Chapter 2

Multi-energy carrier networks

2.1 Background

The electrical network problems caused by the intermittency of the renewable energy production have been widely known for a long time. A lot of research has been done for example on how the voltage control or storage issues should be solved to allow the renewable energy sources to penetrate into electricity systems [1, 2]. More lately the smart-grid aspect that utilizes modern information technology has come into play [3].

Also natural gas lines or district heating and cooling networks have been studied. Heat and mass transfer has been widely investigated [4] as well as different simulation models for the networks [5, 6]. All this research however has considered mainly only one or two energy carrier at a time. The energy system as a whole is still widely unstudied, for example interactions of different energy types and the intertwinement of the networks.

Geidl, Andersson et al. have introduced a multiple energy hub concept [7]. In their work, an energy hub is a unit where different energy carriers are conditioned, converted and stored. They have done optimization studies of how the different procedures inside the hub should be carried out in an efficient way [8, 9]. Their research has been limited to only one hub whereas this thesis tries to widen the inspection to cover the whole networks of different energy carriers.

2.2 Principles and advantages of multi-energy carrier networks

The cornerstone of the thesis is the concept of multi-energy carrier networks. It means that there are multiple different energy networks in a city and that they are intertwined in a smart way. Mainly four different energy types are modelled, electricity, heat, gas and cooling. A city can have networks for them all, electric power grid, district heating and

cooling network and natural gas lines. On top of these, also other types of energy networks, more virtual ones, may be included. For example electric vehicles with their batteries form one type of energy carrier network.

Intertwinement means that the networks are connected to each other nearly everywhere, and not just there where for example the large power plants are situated. Going into details and very small scale, every household could form such an interconnector node between the grids. A household could have a little fuel cell to convert natural gas into electricity or heat, or electric chiller to make cooling out of electricity.

In the model, a city is divided into *nodes* (e.g. blocks or districts of a city), and each one of them has its own energy consumption profile. In the nodes, it is possible to produce, store or convert the energy. In practice, all calculations concerning the energy is carried out in the nodal level. The only exception to this is the transportation of energy, which is done in the networks connecting the nodes.

The concept of multi-carrier networks has many advantages over the traditional way of thinking where different energy types are considered more or less separately. Multi-carrier networks enable one energy type to solve problems in some other energy network. For example, there can be moments in time that the renewable production is too high and the network would not stand the electricity flows needed. In such case, the district heating network could save the situation. Instead of transporting the power as electricity, it could be converted and transported as heat.

Multi-carrier networks enable a bunch of new ways to store energy. A good example is again electricity. Wind and solar power production is very intermittent, and therefore big electricity stores (batteries) would be needed. The battery technology is though very expensive and immature yet for applications large enough. One solution to the problem could be gasification. Hydrogen (gas) could be produced by electrolysis from the excess electricity of wind turbines and easily converted back to electricity during low wind conditions.

The structure and strength of electrical network is a limiting factor when planning the locations of the distributed energy generation. Best places in the grid are the strong trunk lines. With multi-energy carrier networks, the spatial area of such strong locations is broadened.

2.3 Sustainable energy technologies

2.3.1 Wind power

Main components of a single wind turbine and the system connecting it to the electrical network are shown in Figure 2.1. Wind hits the blades and rotates the axis. This rotational energy then goes through a gearbox to a generator. From the generator, the electricity is then

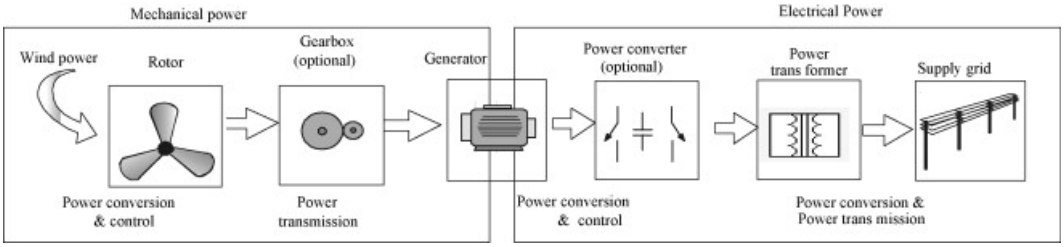

Figure 2.1: Simplified diagram of a wind turbine system [10].

led down to a transformer that sends it to the electrical network. Normally, the turbines can operate in a wind speed range from 3–4 m/s up to about 25 m/s. The flexibility and the sophisticated control systems allow the turbines to maximize their energy production as well as harmonize its operation with the electrical network. [10, 11]

In theory, a turbine could produce electricity with its maximum (name-plate) capacity throughout the year. The ratio of the actual production and the theoretical maximum is called capacity factor. The capacity factors are typically in the range of 20–40 % depending on the technology and location of the turbine [12]. Best located offshore turbines can reach even above this scale.

The challenge with wind power (as several other renewable energy sources too) is its variability. Figure 2.2 shows duration curves of wind power production of a single turbine, whole Denmark and the Nordic countries. The figure shows how the geographical spreading of the wind power production smoothens the duration curve, but still even when considering all Nordic countries as a whole, the fluctuations are huge [13]. The geographical smoothening does not help the situation in the line of the electrical network which a large wind power is connected to. The voltages of such a line can fluctuate dramatically if the wind farm is oversized with respect to the strength of the grid.

As the share of wind power increases, forecasting tools and the predictability of the production become very important. The average error in predicting wind power production (13–37 hours ahead) is 8–9 % in the Nordpool energy market. This is much larger than the average error in load forecasts, 1.5–3 % [13]. The gap between these should be narrowed to ensure reliable and flexible energy system in the future.

The installation of wind power is rather simple practically everywhere in the world. This has been a good boost for wind turbines as the demand for clean energy has grown more and more. Between the years 1998 and 2008, the average cumulative wind power capacity grew globally at the rate of over 30 % a year [14]. At the end of 2010, there was about 197 GW of installed wind power in the world, 84 GW of this in the European Union. The number is seven times more than just ten years ago [15]. China and the United States are also remarkable players in the growing market, both reaching over 40 GW in 2010 [16].

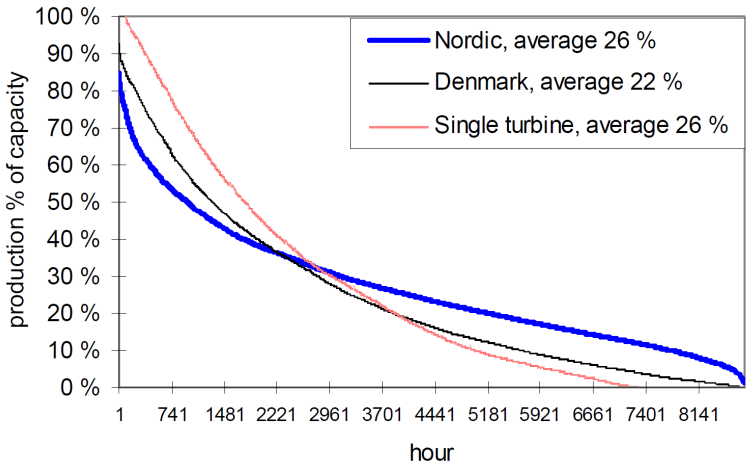

Figure 2.2: Duration curve of wind power and the effect of geographical spreading (data from year 2000). [13]

In 2010, the wind power represented 5.3 % of the gross final electricity consumption in the EU. In Denmark, this figure was as much as 24 % [15]. The future is looking positive. According to the Global Wind Energy Council, wind energy could cover 11.5–12.7 % of global electricity consumption in 2020, and in 2030, the world could reach today's numbers in Denmark by 20.2–24.9 %. The numbers depend on the increase in electricity demand. [17]

More and more electricity is produced by wind power. To be able to produce significant shares in total consumption, small wind farms with 5 or 6 turbines are not enough anymore. In a few years, several farms with maximum output power of about 500 MW and beyond are built and connected to energy systems. One good example of the largest wind farms in the world is in Roscoe, Texas. The total capacity of the Roscoe wind farm is over 780 MW which is produced with 627 turbines [18].

As the number of wind power installations has increased dramatically in recent years, so has done also the size of a single turbine. Wind turbines built today are about one hundred times larger than just 20 years ago (from 25 kW to about 2.5 MW and beyond). The biggest turbine built to date is the Enercon E126 that can produce up to 7.5 MW of electricity [19].

2.3.2 Photovoltaics

Photovoltaic cells (PV) or solar cells are electrical devices that convert the energy of light directly into electricity. The conversion is based on semiconductors and the photovoltaic effect. Most widely used PV cell type is the one based on crystalline silicon. On top of this, many thin-film technologies has developed, for example cadmium telluride, copper indium

diselenide and amorphous silicon sells. Also dye-sensitized and organic solar cells can be included in this list.

Figure 2.3 shows how single cells can be connected to each other to form larger units in support and stand structures. These are called modules. They are often planned to produce the common 12 V voltage. Modules can then be connected in parallel or in series to form an array of desired voltage–current combination. [20]

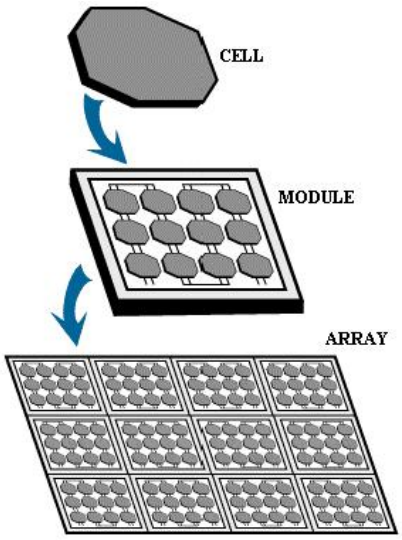

Figure 2.3: Single cells are installed together to form modules and arrays [20].

Solar production is very fluctuating which causes challenges for the energy system. The production is characterized by a strong day–night rhythm as well as seasonal and random variations (e.g. cloudiness of the weather). In the same fashion as with the wind power, the forecasting of the production is essential in energy markets, and even though the daily and seasonal variations are regular and completely predictable, the challenge in forecasting is the random fluctuation caused by weather conditions.

An advantage of solar cell technology is that the cells can be integrated in the built environment, rooftops, windows etc. (BIPV, building-integrated photovoltaics). This brings distributed generation right on the place where the electricity is consumed. The sizes of BIPV installations vary from a few kilowatts to about one megawatt. On top of the BIPV solutions, also large PV power stations have been connected to the energy system recently. Their sizes today are in the range of 25–100 MW, but even larger ones have been planned.

As in wind power, also in solar cells the global growth rates have been huge in recent years. In 2010, there were almost 40 GW of installed PV power and that produces about 50 TWh of electricity. These numbers are about 2.5 times higher than just two years before and seven times higher than in 2005 (Figure 2.4). The EU is the market leader since approximately 75 % of world's PV production lies in Europe.

European Photovoltaic Industry Association has forecasted that the installed PV capacity will continue its rapid growth, and that in 2015, the cumulative capacity could be some 130–200 GW, depending on the policies of the countries. The fastest development is expected in China and North America. They are about to increase their capacity by more than 10-times over the present situation. In China, the capacity can grow to even 20 times larger. [21]

As the PV technology has been developing, the costs of PV produced electricity has come

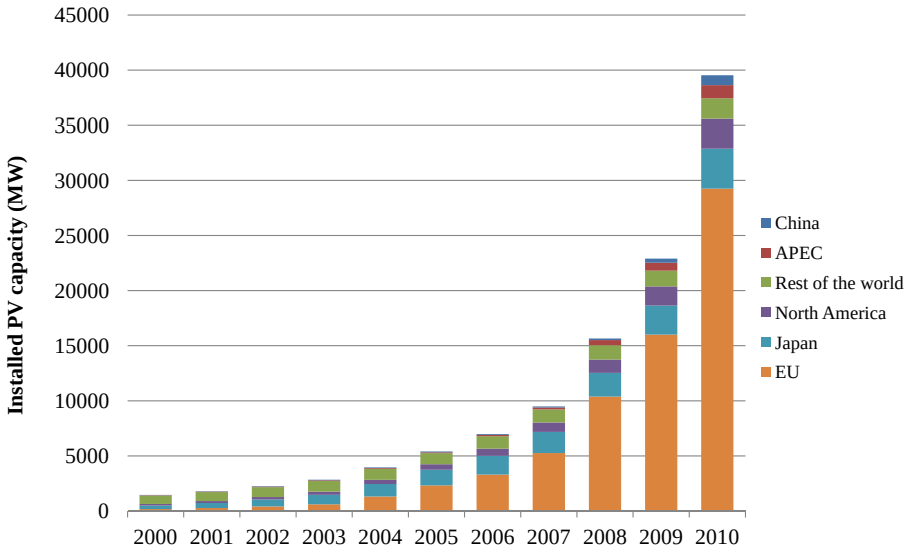

Figure 2.4: Development of the cumulative installed PV capacity in the world [21]. APEC means Asia-Pacific region countries that include South Korea, Australia, Taiwan and Thailand.

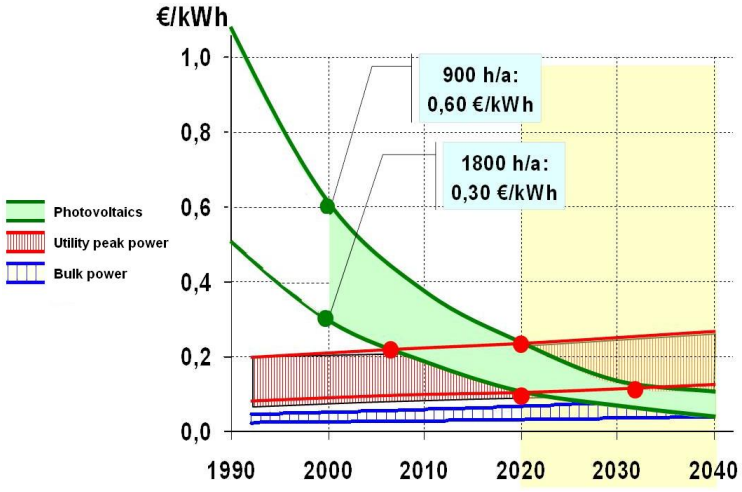

Figure 2.5: The predicted development of PV and utility electricity prices [22].

down. In 2004, it was estimated that grid parity (time when PV electricity costs are at the same level as the one of other sources) will be achieved in 2020–2030, momentarily in the most sunnier places maybe already in the beginning of 2010s (Figure 2.5) [22]. And indeed, first reports from for example Australia now tell that grid parity could have been achieved [23].

2.3.3 Micro-CHP and trigeneration

Micro combined heat and power (micro-CHP) is a technology where heat and power demands of a single household, office building or a block of them are satisfied with one production unit system. A good example of this is a fuel cell or a gas turbine that produces electricity for the building but at the same time produces heat. Normally, this heat would be wasted but in micro-CHP systems it is gathered or stored and then utilized. The gathered energy may heat up the building or its domestic hot water.

Trigeneration is a term that describes energy production in which also cooling is produced at the same time with heat and electricity. It is sometimes called also combined heat, cooling and power (CHCP) production. There is a schematic illustration of a trigeneration system in Figure 2.6.

Especially solid oxide fuel cells (SOFC) are a good option as the main energy source of a trigeneration plant because they operate in very high temperatures (600–1000 °C) and thus produce very high-grade (i.e. hot) heat. The high-grade heat may be led to an absorption chiller to be converted into cooling energy or directly used in heating systems. The high temperature makes it possible to utilize the waste heat to a great extent. Total efficiencies of even 80 % are possible [24].

Solid oxide fuel cells are electrochemical devices that convert chemical energy straightforwardly into electricity and heat. There is an schematic representation of the operation principle of the cell in Figure 2.7. Fuel (typically hydrogen or natural gas) is led to an anode where it get oxidized and sends electrons to an external circuit. At the same time oxygen (pure O_2 or air) is reduced at a cathode, i.e. it receives electrons from the external circuit

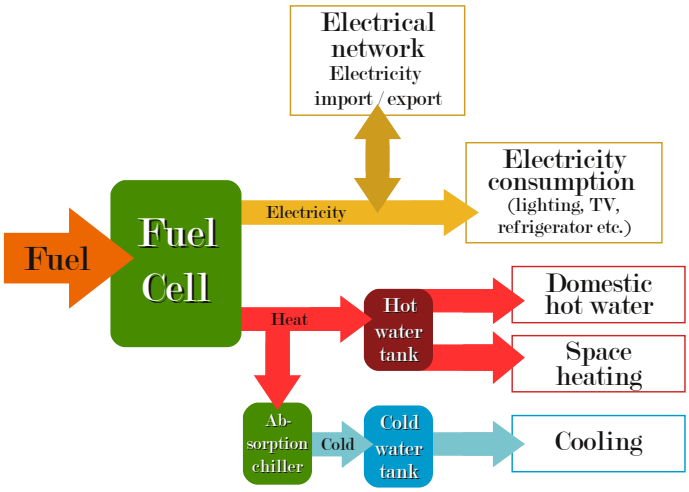

Figure 2.6: An example of a trigeneration system.

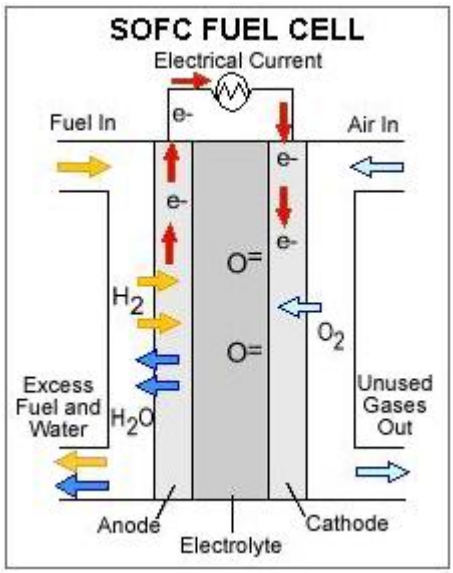

Figure 2.7: Operation principle of solid oxide fuel cells. [25]

and oxygen ions (O^{2-}) are formed. These ions travel through the electrolyte layer to the anode side, where they react with hydrogen ions and form water. Electrolyte between the electrodes does not conduct electrons, which is why they are compelled to travel through an external circuit and electricity is born.

Fuel cells have several advantages, for example they do not necessarily produce any pollutions. The only exhaust is water if hydrogen is used as fuel. Secondly, there is no burning process in fuel cells, which means that there is no Carnot limit for efficiency. Third main advantage is that they are flexible in many sense. The power is easily scalable, it can be increased by adding more cells into one stack. The variety of fuels is also wide. On top of the hydrogen, also different types of carbon compounds can be used, for example carbon monoxide or hydrocarbons. Furthermore, the cells have no moving parts which makes them silent and also very little mechanical degradation can occur.

High operating temperature places requirements for significant thermal shielding around the cell and results in a slow start-up. Hot temperatures require also very durable materials. The main technical challenge in SOFC industry is thus the development of cheap and durable materials [25].

Absorption chiller is a thermochemical device that uses heat to produce cooling. There is a simplified diagram of it in figure 2.8. The operation is based on boiling at very low pressure where the boiling point is also low. The chiller needs two different substances, refrigerant and absorbent (e.g. ammonia and water respectively). The heat (that drives the cycle) makes the refrigerant to boil out of the refrigerant–absorbent solution. This happens under pressure in a generator. The hot refrigerant vapour is passed through a cooling coil

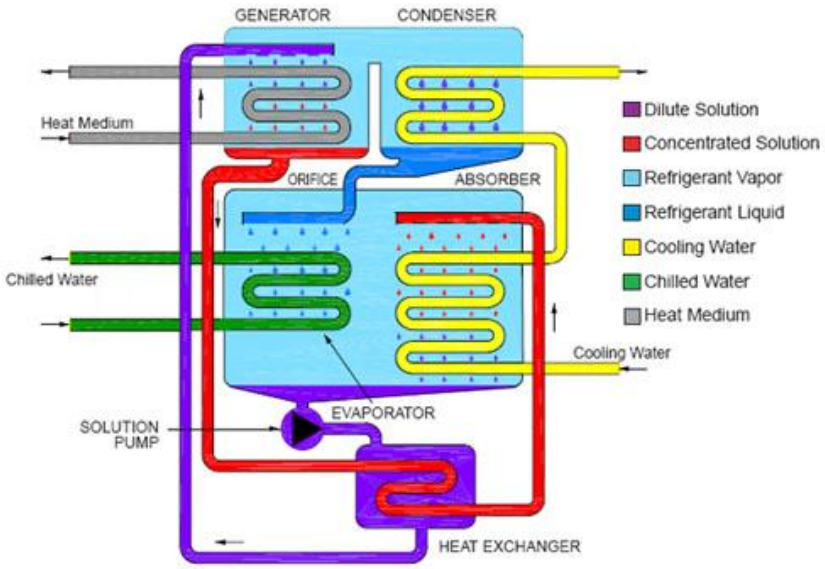

Figure 2.8: Cycle diagram of an absorption chiller [26].

and condenses into liquid. The liquid refrigerant is then evaporated at very low pressure and the cooling effect is achieved, because the energy required for boiling is taken from the surroundings (i.e. the water that is flowing through to be cooled down). The name of the chiller comes from the absorption process after the boiling. There, the refrigerant vapour is absorbed back to the absorbent and the cycle is ready to be repeated.

The sizing of trigeneration plants may vary from a few to about one hundred kilowatts, depending on the type of the fuel cells. With SOFC technology, it is possible to achieve the 100 kW scale, and even more [27].

Trigeneration has one huge advantage over the wind and solar power, its controllability. For this reason, it would also be an interesting option to operate such a system together with those renewable energy sources. It could be turned on when other production is low and vice versa. During the operation, it could charge thermal storage, and the stored energy can be utilized when the system is off.

Trigeneration suites well in built environments and especially places where the cooling load at summer and heating load at winter are relatively high. As electricity load keeps comparatively stable throughout a year (or at least the yearly variation is much smaller compared to cooling and heating), it is favourable that there is always some thermal by-product of electricity to be produced. This way the efficiency and utilization degree of the system stay always at high level.

2.3.4 Plug-in electric vehicles

Since the transport sector is responsible for 25% of the world's emissions [28], it is important that the worldwide road traffic could be turned into electrical. All-electric vehicles are beginning to come to market but their short operation distances decrease their attractiveness. This example shows that the main technical challenge with electric vehicles (EV) and their market penetration is the battery technology. Lithium-ion batteries used today with EVs, are still too expensive and have too low energy density. They are also the main reason for the high prices of the vehicles. [29]

Before all-electric vehicles become competitive with combustion engine cars, plug-in hybrid electric vehicles (PHEV) offer a good intermediate step towards less polluting traffic system. PHEVs are hybrid vehicles that have rechargeable batteries to store energy. The batteries are charged by connecting the car to an external electricity source (usually electrical grid). Contrary to all-electric vehicles, plug-in hybrids have also internal combustion engine on top of the electric one. This engine can be used as in normal hybrid vehicles, where the electric power train is installed to achieve better fuel economy and less emissions.

Although plug-in hybrids won't make the traffic completely fossil fuel free, they are an important step towards all-electric vehicles. The fuel consumption is radically smaller than the one of the normal combustion engine vehicles. For example Toyota Prius Plug-in Hybrid that goes on sale in early 2012, consumes only 2.2 l/100 km when driving with hybrid mode [30]. All-electricity mode offers of course zero consumption. Diesel hybrid Volvo V60 Plug-in promises only 1.9 l/100 km [31]. Carbon dioxide emissions are only 49 g/km in both cars.

The main principle of PHEVs is to drive first with electricity only and if the batteries are depleted, the combustion engine is turned on. There are different techniques to accomplish this. The engine and electricity may be used in combination to produce the propulsion for the wheels. In some vehicles (called extended range electric vehicles), combustion engine is used only to charge the electric batteries without driving the wheels directly. Extra charging of the batteries is also achieved by regenerative braking, in which the kinetic energy of the wheels is converted back to electricity.

If the driving distance is small, it is possible to drive the whole trip with electricity only. Most of the car use is for short home-to-work type of trips. In Finland, 80 % of the trips made by private cars are shorter than 20 km [32]. All these trips could be easily driven with electricity only, especially if the charging is possible between the trips. Person living close to his or her work place, wouldn't have to burn any fossil fuel in normal every-day use. This means that plug-in hybrids, even with relatively short all-electric range, could transform the traffic into dramatically less polluting.

Plug-in hybrids can be charged from the normal wall socket with normal 230 V (or 120 V) grid voltage. In Finland, the required recharging infrastructure is rather ready, since there are sockets for preheating the cars installed in many parking lots. These could be used also with PHEV charging. The problems may occur when recharging the vehicles quickly with high power, and if the grid is not strong enough. This is why different smart grid applications are being developed. The target is to control the grid load so that it would never rise too high.

PHEVs are interesting also by offering an option for grid stabilization. With smart charging/discharging strategies, it could be possible to level out the fluctuations in network load. In this scenario, PHEV batteries would be used as short-term electricity storage. The recharging could be timed to the moments of high production, and when the production is low, the energy in the batteries could be feed into the grid. More stable grid load would mean more reliable network and more predictable energy market behaviour.

Chapter 3

Description of the model

The thesis and the used model is based on power (kW, MW) and energy (kWh, MWh) and no network voltages, pressures or temperatures are considered as such in the code. This way, the connections and interactions between the networks are as simple as possible and the different forms of energy are easily comparable with each other. If one wants to calculate for example the voltages in the electrical network, it can be done afterwards when the transported amounts of energy and power are known [33].

The MATLAB® model is completely based on the model described in [34]. The documentation and more thorough description of the MATLAB® functions, their input and output parameters are explained there. This chapter discusses the energy questions and phenomena behind the MATLAB code. It shows what type of simulations can be run and also clarifies the calculation principles.

3.1 Energy networks and energy profiles

3.1.1 City energy networks

The overall area of a city is modelled with a square, the size of which depends on the size of the city in real world. This large square is divided into several smaller squares called nodes. In practice, all calculations are carried out at the nodal level. It is also possible to divide one of the nodes into subnodes, for example a node of size 1 km $\times$ 1 km could be divided into one hundred 100 m $\times$ 100 m nodes.

The nodes are connected to each other with different energy networks. The model can include maximum of four different networks at a time, for example *electricity*, *heat*, *gas* and *cooling*. There is its own network for each energy type, and it does not need to follow the other networks in any way.

Every network must have a base node (or an interconnector node). The base node con-

nects the network to an upper-level energy transportation grid. In the electrical network for example, the base node means the transformer connecting the urban distribution network to national transmission lines. The base node delivers all the energy needed (but not produced) within the area. Also, if there is more production than consumption, the base node receives the extra energy that is not consumed or stored. If no upper transmission level exists (for example with local district heating network), the base node may be used just to find out the energy imbalances of the whole city.

It is important that the networks do not have any loops and that every node is connected somewhere. This means that if there is no heating network in the city but heating is studied in the simulation, there has to be a heating network in the model. In such a case, the network is purely virtual, and the calculations can be run so that no energy is put to flow there.

To create the networks, two different strategies were considered. Both of them are based on the direct Euclidean distance from a node to the base node. The node is connected to the neighbouring node that is either closest or second closest to the base node. If there are two possible options, the node is chosen by random. In the latter strategy (connecting to the second closest), the second closest and third closest nodes may be at the same distance. In this case, the closest node is chosen instead of these two. The differences of these two strategies can be seen in Figure 3.1.

For the case studies, the networks were created by connecting the nodes to the neighbour second closest to the base node (right one in Fig 3.1). No accurate data was available on the network structures of the studied cities. However, there is no big difference between the strategies. The total length of the network is same using both strategies. The chosen

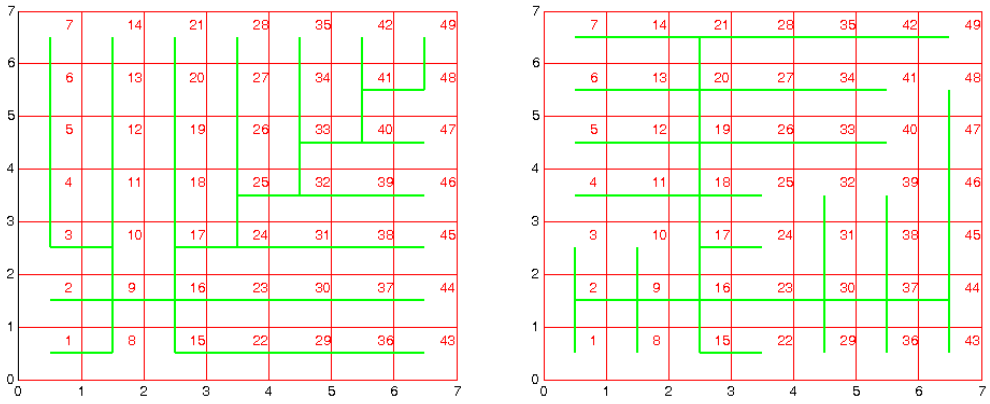

Figure 3.1: Two different networks. The left one is created so that the nodes are connected to the neighbour closest to the base node (16) and the right one so that the connection is to the neighbour second closest to the base node.

strategy was picked up mainly because it creates networks with more visually prominent division between strong trunk lines and side branches.

3.1.2 Hierarchy of nodes

In a loopless network, the nodes have a hierarchy between themselves. Terms master, slave, upstream and downstream are used later in this thesis. Figure 3.2 clarifies these terms. Master is the neighbouring node that is the next one in line towards the base node. The whole line is called upstream. Slaves are the other neighbouring nodes, i.e. those that are pointing away from the base node. Downstream includes in addition to the slaves, also slaves' slaves, their slaves and so on.

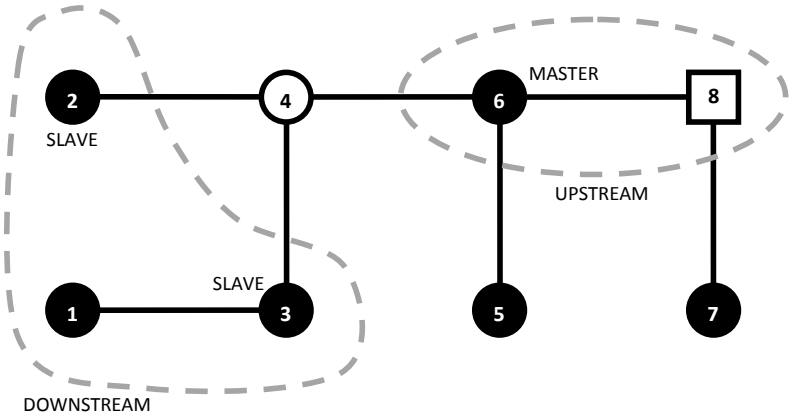

Figure 3.2: Hierarchy of the nodes. The terms are related to node 4 (white circle). Node 8 (white square) is the base node.

3.1.3 Dividing consumption profiles among the nodes

Normally, energy consumption data is available only for the city as a whole. Thus this data has to be distributed to the nodes. It is possible to do it manually for each node, but this may be tedious and troublesome. A faster way of creating the node-wise consumption profiles was developed. It is based on the city model where the office buildings are located closely in the city center and manufacturing industry some dozens of kilometres away from there, actual distance depends on the size of the city. Homes are distributed more equally throughout the city.

Three different consumer types were considered: office, manufacturing and households.

The density d_i of the consumer type i is modelled with Gaussian function

$$d_i(\mathbf{r}) = d_{0,i} e^{-\alpha_i (|\mathbf{r}|_{\mathrm{cc}} - r_{0,i})^2} \tag{3.1}$$

In above equation, $d_{0,i}$ is the maximum density, α_i positive constant describing the width of the density distribution and $r_{0,i}$ is the distance from the city center at which the density is peaked. Notation $|\mathbf{r}|_{\mathrm{cc}}$ means the distance of the point $\mathbf{r}$ from the city center (cc).

On top of the spatial distribution of consumer types (Equation 3.1), also a temporal base profile $h_i(t)$ is needed for each consumer type i. This describes how the load of a one consumer (of the type considered) is distributed temporally over the whole simulation time. The consumer type-wise consumption profile $q_i(\mathbf{r}, t)$ is then

$$q_i(\mathbf{r}, t) = d_i(\mathbf{r}) h_i(t) \tag{3.2}$$

This equation shows that the units of d and h should be compatible in a way that the unit of $q_i(\mathbf{r}, t)$ is MW. If the densities are measured with unit 'persons/area', the temporal base profiles should be scaled so that it describes the average load of one person. To get the total consumption Q of the node n at time step t, one must sum all the consumer types together:

$$Q_n(t) = A \sum_{i=1}^{3} q_i(\mathbf{r}_n, t) \tag{3.3}$$

where A is the area of the node and $\mathbf{r}_n$ means the coordinates of the center point of the node n. After calculating node-wise profiles Q_n, one has to check that their sum at every time step matches with the one of the whole city Q_{city}. If this is not the case, the node-wise profiles Q_n has to be scaled to a correct value. The correct scaled profile $Q'_n(t)$ is thus found out by

$$Q'_n(t) = Q_n(t) \frac{Q_{\mathrm{city}}(t)}{\sum_k Q_k(t)} \qquad \forall\, n, t \tag{3.4}$$

The process above is repeated for all energy carriers. The densities d_i are the same but the temporal base profiles h_i may be totally different.

3.2 Energy balances in the nodes

The goal of this section is to describe different methods how the node-wise energy balances D are calculated (the letter D comes from 'power to be Distributed'). The calculations are based on the node-wise production and consumption data, P and Q respectively. Their difference is called *net production* N. (From now on, the time step is marked as superscript

instead of the brackets i.e. $P_n(t) = P_n^t$.)

$$N_n^t = P_n^t - Q_n^t \tag{3.5}$$

The simplest method to run the simulation is to ignore all storing or conversion possibilities and use N as D

$$D_n^t = N_n^t \tag{3.6}$$

The above equations shows that when D has a positive value, the node does not need all the energy it produces. Respectively, negative values show that the node is not producing enough and it needs to import energy from the network.

3.2.1 Conversion

Conversion between the energy types enables their mutual interaction and makes the model a multicarrier model. There are many different ways and technologies to actually do the conversions, electric heaters, micro-CHP, boilers etc. In spite of the wide technology spectrum, model-wise though the principles how the conversions are carried out, are the same. One needs to define the conversion efficiencies or coefficients of performance (COP) between the energy carriers. Those are marked with $\eta_{a \triangleright b}$ where a is the energy carrier that is converted into energy b.

When converting z MW of energy type a into energy type b at node n and at time t, the equations are

$$\begin{cases} C_{a,n}^t = -z \\ C_{b,n}^t = \eta_{a \triangleright b}\, z \end{cases} \tag{3.7}$$

where $C_{a,n}^t$ and $C_{b,n}^t$ means the amount of converted energy. Negative value means that energy is converted into some other type, and positive one that some other energy type is converted into that type. Conversion affects the net production in Equation 3.5, and with the conversion term it looks like

$$N_n^t = P_n^t - Q_n^t + C_n^t \tag{3.8}$$

The rules, when the conversion is done and between which energy types, depend on the studied case. They are made clear in Chapter 4 when different conversion cases are represented.

3.2.2 Storage

Storage makes it possible to control and modify the temporal behaviour of the energy system. It is a way to transport the energy not spatially but temporally. The model includes two different ways of local energy storage, *straight* and *limited*. They both are based on the idea that before exporting energy to the network (or importing it from there) the state of the stores is checked. If there is surplus energy production after the consumption and conversion needs of the node are satisfied ($N_n^t > 0$) and there is storage capacity free, the energy is stored. The same applies also for the energy deficits ($N_n^t < 0$). Satisfying the deficit from the stores is preferred to doing that from the network. This way, the network comes into play only at the moments when the storage capacity is not sufficient for the energy imbalances.

In the straight storage method, all the energy that is possible to be stored, is stored. The only limit is the storage capacity (how much energy fits in). In the same way, it is possible to take all the energy out of the store if needed. The amount of energy (MWh) in the store at tth time step (S^t) can be calculated if the state of the store at the previous time step is known:

$$S_n^t = \begin{cases} \min\left\{S_n^{t-1} + N_n^t \Delta t,\ \ S_{\max,n}\right\}, & \text{if } N_n^t > 0 \ \text{ (charge)} \\ \max\left\{S_n^{t-1} + N_n^t \Delta t,\ \ 0\right\}, & \text{if } N_n^t < 0 \ \text{ (discharge)} \end{cases} \tag{3.9}$$

where Δt is the length of the time step (1 h in this thesis) and $S_{\max,n}$ the maximum amount of energy that fits in the store at node n.

In the limited method, there are limitations concerning how much energy it is allowed to take out of the store or to put into there. The limitations are implemented by two extra coefficients x_{in} and x_{out}. They tell how big share of the energy in store (or the free storage capacity) can be utilized. For example, if x_{in} = 0.5 and the store is half full, it is possible to charge the store only up to 75 %. Thus, only half (x_{in}) of the free capacity is utilized. With the limitations, Equation 3.9 can be written as

$$S_n^t = \begin{cases} S_n^{t-1} + \min\left\{N_n^t \Delta t,\ \ x_{\text{in}}\left(S_{\max,n} - S_n^{t-1}\right)\right\}, & \text{if } N_n^t > 0 \ \text{ (charge)} \\ S_n^{t-1} - \min\left\{\left|N_n^t\right| \Delta t,\ \ x_{\text{out}} S_n^{t-1}\right\}, & \text{if } N_n^t < 0 \ \text{ (discharge)} \end{cases} \tag{3.10}$$

Equations 3.9 and 3.10 assume that the charging, discharging and keeping the energy in the store happen with efficiency of 100 %. If this is not the case, one could add the efficiency factors into the equations:

$$S_n^t = \begin{cases} \min\left\{\varsigma S_n^{t-1} + \varsigma_+ N_n^t \Delta t,\ \ S_{\max,n}\right\}, & \text{if } N_n^t > 0 \ \text{ (charge)} \\ \max\left\{\varsigma S_n^{t-1} + \frac{1}{\varsigma_-} N_n^t \Delta t,\ \ 0\right\}, & \text{if } N_n^t < 0 \ \text{ (discharge)} \end{cases} \tag{3.11}$$

$$S_n^t = \begin{cases} \varsigma S_n^{t-1} + \min\left\{\varsigma_+ N_n^t \Delta t,\ \ x_{\text{in}}\left(S_{\max,n} - \varsigma S_n^{t-1}\right)\right\}, & \text{if } N_n^t > 0 \ \text{ (charge)} \\ \varsigma S_n^{t-1} - \min\left\{\frac{1}{\varsigma_-}\left|N_n^t\right|\Delta t,\ \ x_{\text{out}}\varsigma S_n^{t-1}\right\}, & \text{if } N_n^t < 0 \ \text{ (discharge)} \end{cases} \tag{3.12}$$

where ς, ς_+ and ς_- are the efficiencies of keeping energy in the store, charging the store and discharging the store, respectively. The difference between the efficiency factors in front of the N_n^t (ς_+ versus $\frac{1}{\varsigma_-}$) is because in the charging, the energy impact to the store is *smaller* than the amount of energy that is originally tried to be stored (all of N_n^t does not go to the store but some of it is lost), respectively in the discharging, *more* energy is needed to take out of the store than finally is used, because a part of it is lost before the use.

The efficiencies under 100 % mean that part of the energy is wasted (W). The amount of it is

$$W_n^t = (1-\varsigma)S_n^{t-1} + \begin{cases} \left(\frac{1}{\varsigma_+} - 1\right)\left(S_n^t - \varsigma S_n^{t-1}\right), & \text{if } N_n^t > 0 \ \text{ (charge)} \\ (1-\varsigma_-)\left(\varsigma S_n^{t-1} - S_n^t\right), & \text{if } N_n^t < 0 \ \text{ (discharge)} \end{cases} \tag{3.13}$$

The first term of the sum are the losses that occur when the energy is kept in the store and the second term relates to charging and discharging. After the losses and the amount of stored energy is known, it is possible to define how much energy may be distributed away from the node:

$$D_n^t = \begin{cases} N_n^t - \frac{1}{\varsigma_+ \Delta t}\left(S_n^t - \varsigma S_n^{t-1}\right), & \text{if } N_n^t > 0 \ \text{ (charge)} \\ N_n^t + \frac{\varsigma_-}{\Delta t}\left(\varsigma S_n^{t-1} - S_n^t\right), & \text{if } N_n^t < 0 \ \text{ (discharge)} \end{cases} \tag{3.14}$$

3.3 Energy flows

After the balances D are calculated for every energy type, energy flows F in the networks are found out. At this point no conversion or storing questions need to be pondered any more, it is done already before defining the final values of Ds. All energy carriers can be calculated with the same principles.

The sign of the flow tells which direction the energy in the line is flowing to. If the flow is positive, the energy is flowing downstream (towards the tails of the grid), and respectively negative flows mean that energy is flowing upstream (towards the base node).

$$\begin{cases} F < 0 & \Rightarrow \quad \text{Energy flows upstream (towards base node)} \\ F > 0 & \Rightarrow \quad \text{Energy flows downstream} \end{cases} \tag{3.15}$$

Calculating the flows is simple. The amount of energy needed to be transported through a line is the sum of the energy needs of the downstream nodes. Thus, the flow of the line l

at time t is

$$F_l^t = - \sum_{n \in \mathrm{ds}(l)} D_n^t \tag{3.16}$$

The notation $\mathrm{ds}(l)$ means all the nodes downstream from the line l. The minus sign in the equation is needed to make the flow to follow the rules in Formula 3.15. The flow from the base node to the outside world can be calculated in the same way as the flows in normal lines, with the Equation 3.16. In that case, the summation is just taken over all the nodes in the grid. This *base node flow* tells in practice the energy balance of the whole city area.

Equation 3.16 assumes that the energy needed to be transported downstream equals to the energy balance of the downstream nodes. This assumption neglects the losses that occur when transporting the energy (so called *flow losses* that are described later). The needed flow should be a bit more than the value given by the equation. The advantage of the assumption is that all numerical iteration loops in the flow calculations are avoided, and thus the calculation routine stays very simple and fast but also accurate enough.

3.3.1 Energy flow channels and overflows

The transportation capacity of the networks is limited. The strength of the network is essential when planning where extra energy production and consumption can be located (without strengthening the network). This thesis assumes that the networks are able to transport the same amount of energy in both directions, upstream and downstream. The limits of the transportation are called *a flow channel* Φ. The absolute value of the flow in the line l should be smaller than the corresponding channel:

$$\left|F_l^t\right| \leq \Phi_l \qquad \forall\, t \tag{3.17}$$

If Equation 3.17 does not hold at some time step, the flow exceeding the channel is called *overflow* $\hat{F}$.

$$\hat{F}_l^t = \begin{cases} \max\left\{0,\, F_l^t - \Phi_l\right\}, & \text{if } F_l^t \geq 0 \\ \min\left\{0,\, F_l^t + \Phi_l\right\}, & \text{if } F_l^t < 0 \end{cases} \tag{3.18}$$

Overflows somewhere in the grid mean that the network is not sufficient to transport all the energy that is required. These problems should be solved either by strengthening the network or by modifying the production/consumption of the nodes downstream from the overflow line. The sign of $\hat{F}$ tells whether there are too much energy flowing upstream or downstream (see Formula 3.15).

In this thesis, flow channels are defined according to reference cases that reflect the situation in the cities at present. The flow channel is set to the maximum value of the flow in a

one-year simulation of the reference case (ref).

$$\Phi_l = \max_t \left| F^t_{l,\mathrm{ref}} \right| \tag{3.19}$$

This means that the networks in the cities are sized exactly so that they survive from the present yearly consumption profiles but no higher flow peaks. Defining the channels like this, is a good way to make comparisons with different energy scenarios and the reference case. This approach also targets to cases where the networks are not put under any more stress than at the moment.

3.3.2 Energy flow losses

At the same time as the flows are calculated, also the losses in the lines are found out. The calculating principles of the flows of different energy types were the same, but for the losses they are not. This is due to different physical phenomena behind the losses.

Electricity. The loss of electrical power in the cable l ($L_{e,l}$) is proportional to the square of the electric current I in the line and thus also to the square of the flowing power F_e

$$L_e = RI^2 = \frac{R}{U^2} F_e^2 \tag{3.20}$$

where R, I and U are the resistance, electric current and voltage of the line. The above equation may be written as

$$L_{e,l} = \kappa_l F_{e,l}^2 \tag{3.21}$$

Here the sub-index e refers to electricity and κ is the loss coefficient that can be scaled in the simulation so that the overall losses throughout the year and in the whole city, match with the real values in some well-known reference case.

Heat. Two factors cause the losses in the district heating network. They are the temperature difference between the hot water in the network and the ground, and pumping the water to flow. Based on the literature [35], the pumping losses can be neglected when inspecting the situation from the power system point of view. Thus only temperature-caused losses are considered here.

At summer time when outside temperatures are warm and heating demand is small (in practice only domestic hot water), the energy flows in the network are regulated by increasing (decreasing) the water flow. At winter when the heat demand may become huge, increasing the water flow is not enough anymore, but one have to raise the temperature of the water too. Then also the heat radiation from the pipes to the ground (i.e. losses) becomes stronger. Because the variables that affect the losses, the temperature and the mass flow, are not controlled separately for every line, the heat losses are calculated for the whole network

at once:

$$L_h^t = \begin{cases} \tilde{L}_h, & \text{if } F_{h,\text{tot}}^t < F_0 \\ \lambda F_{h,\text{tot}}^t, & \text{if } F_{h,\text{tot}}^t > F_0 \end{cases} \tag{3.22}$$

$\tilde{L}_h$ is the minimum energy that is lossed in the network at each time step even if no heat energy is used (water stands idle in the pipes and cools down). λ is a constant coefficient and F_0 the energy flow after which the temperature of the water in the pipes has to be increased. The value of L_h^t must be unambiguous when $F_{h,\text{tot}}^t = F_0$ which why

$$\tilde{L}_h = \lambda F_0 \tag{3.23}$$

The two free parameters (λ and F_0) can be chosen so that the overall losses match with the realistic values of the reference case.

If one wants to know how the losses are approximately divided between the lines, one must take into account that the pipes have different diameters. Hagen–Poiseuille equation states that the mass flow rate φ in the pipe is proportional to the fourth power of the pipe radius ρ [36]

$$\varphi = \frac{\pi \Delta p}{8 \nu s} \rho^4 \tag{3.24}$$

where Δp is the pressure difference between the ends of the pipe, ν is kinematic viscosity and s length of the pipe. If the temperature in the pipe stays constant the transported energy flow F is directly proportional to the mass flow. Because of the assumption that the pipes are sized according to the maximum flows (i.e. flow channels Φ_l), it must hold for the radius in line l

$$\rho_l \sim \sqrt[4]{\varphi_{\max,l}} \sim \sqrt[4]{\Phi_l} \tag{3.25}$$

The losses depend on the surface area of the pipe A_p which is directly proportional to the radius. Using 3.24 and 3.25 one gets

$$L_{h,l} \sim A_{p,l} \sim \rho_l \sim \sqrt[4]{\Phi_{h,l}} \tag{3.26}$$

$$L_{h,l} = k_h \sqrt[4]{\Phi_{h,l}} \tag{3.27}$$

where k is a scaling factor that has to be adjusted so that the overall losses in the pipes match the one of the whole grid (L_h in Equation 3.22):

$$L_h = \sum_l L_{h,l} \tag{3.28}$$

Cooling. Cooling losses are based on temperature differences too. It is assumed that the district cooling network is strong enough so that all differences in cooling demand can be

met by adjusting the water flow. This means that the temperature of the cold water in the pipes stays always constant and thus the losses are constant and do not depend on time

$$L_c^t = L_c \tag{3.29}$$

In the same way as with heat, the overall losses can be divided for every single line by examining the flow channels. Equations similar to 3.27 and 3.28 can also be deduced for cooling:

$$L_{c,l} = k_c \sqrt[4]{\Phi_{c,l}} \tag{3.30}$$

$$L_c = \sum_l L_{c,l} \tag{3.31}$$

Gas. The thesis assumes that no gas escapes from the pipes when it is transported. Thus the gas losses are zero by definition:

$$L_{g,l}^t = 0 \qquad \forall\, l, t \tag{3.32}$$

3.4 Tracking energy flows in the networks

This section presents a way to find out answers to two questions.

- Where is the energy produced, which is consumed at node n?
- Where does the energy, which is produced at node n, flow to?

The answer to the latter question is a column vector $\mathbf{y}_n$ of length $\mathcal{N} + 1$, where $\mathcal{N}$ is the number of nodes in the grid. The ith element tells how much node-n-produced energy (in MWh) is consumed at node i. The last element ($\mathcal{N} + 1$) represents the outside world, i.e. how much energy comes through the base node from outside the grid.

Calculation is started from the node n, and continued by examining all the nodes where the flows transport energy from there. During the calculation, data about the nodes that still have to be calculated must be stored somewhere, so that all nodes in lines also with many branches are calculated. Calculation algorithm (that considers only one specific time step) to find $\mathbf{y}_n$ is as follows:

1) Check the value of D_n. If it is negative, no energy can flow outside the node, and all node-n-produced energy is consumed locally at node n. The calculation can be stopped and $\mathbf{y}_n$ has only one non-zero element, nth one that has value P_n. If D_n is however positive, energy gets to flow in the grid, the value of the nth element of $\mathbf{y}_n$ is Q_n and the calculation has to be continued.

From now on some general node x in the calculation routine is considered. An assumption is made that there are k incoming flows $F_1, \ldots, F_k$ and m outgoing flows $G_1, \ldots, G_m$.

2) Find out the incoming flows $F_1, \ldots, F_k$. Each of them has a composition

$$\mathbf{F}_i = [f_i^{(n)} \;\; f_i^{(-n)}] \tag{3.33}$$

so that $|F_i| = f_i^{(n)} + f_i^{(-n)}$. Here $f_i^{(n)}$ is the energy that is produced at node n and $f_i^{(-n)}$ is produced somewhere else. The composition for the flow coming from the direction of node n is known because of step 5 in the previous iteration rounds. For the rest incoming flows the value of $f_i^{(n)}$ is 0 and the composition is $\mathbf{F}_i = [0 \;\; |F_i|]$. Total incoming flow to node x is now

$$F_{\text{in}} = \sum_{i=1}^{k} |F_i| \tag{3.34}$$

that has a composition

$$\mathbf{F}_{\text{in}} = \sum_{i=1}^{k} \mathbf{F}_i = \left[\sum_{i=1}^{k} f_i^{(n)} \;\; \sum_{i=1}^{k} f_i^{(-n)} \right] \tag{3.35}$$

3) Similarly to incoming flows, also energy balance D_x of the node is divided into a two-component vector (the first element refers to node-n-produced energy and the second one to energy produced somewhere else):

$$\mathbf{D}_x = \begin{cases} [0 \quad D_x], & \text{if } x \neq n \\ [D_x \quad 0], & \text{if } x = n \end{cases} \tag{3.36}$$

4) If $D_x < 0$, node x consumes energy from the grid (and part of that energy comes from the node n). The amount of this energy is

$$Q_{\text{grid}} = \begin{bmatrix} q^{(n)} & q^{(-n)} \end{bmatrix} = \frac{|D_x|}{F_{\text{in}}} \mathbf{F}_{\text{in}} \tag{3.37}$$

Vector $\mathbf{y}_x$ can be updated. The xth element of it gets value $q^{(n)}$.

5) The compositions of the outgoing flows G_i are calculated:

$$\mathbf{G}_{\text{out}} = \mathbf{F}_{\text{in}} + \mathbf{D}_x \tag{3.38}$$

$$\mathbf{G}_i = \frac{G_i}{\sum_{j=1}^{m} G_j} \mathbf{G}_{\text{out}} \tag{3.39}$$

6) Take the next node and go to step 2. This procedure is continued as long as there are still nodes to be calculated.

After repeating the procedure for every node, one should have $\mathcal{N}$ vectors $\mathbf{y}_1, \ldots, \mathbf{y}_\mathcal{N}$, each one of them telling the destination distribution of the energy produced at the corresponding node. To find out where the energy comes from that is consumed at a specific node, the vectors can be arranged in a matrix

$$\mathbf{Y} = [\mathbf{y}_1 \quad \mathbf{y}_2 \ \cdots \ \mathbf{y}_\mathcal{N} \quad \mathbf{y}_{\mathcal{N}+1}] \tag{3.40}$$

The last column ($\mathcal{N}+1$) is for the outside world (i.e. how much energy comes from outside the grid). It cannot be obtained from the calculation routine above, but has to be calculated separately. The jth element of it is:

$$\mathbf{y}_{\mathcal{N}+1}^{(j)} = Q_j - \sum_{i=1}^{\mathcal{N}} \mathbf{Y}_i^{(j)} \tag{3.41}$$

where Q_j is the consumption of the node j. The ith horizontal row of $\mathbf{Y}$ tells where the energy to the node i comes from.

3.5 Linking electric vehicles to the model

From now on, terms *electric vehicles* and *EVs* refer always to plug-in hybrid vehicles, which was the technology studied here. EVs can be considered both energy storages and energy carriers. In this thesis, they are used mainly for modifying the local production/consumption profiles in the nodes. For example, if solar panels are producing too much electricity on a sunny day, EVs could be told to recharge so that the local production does not have to be fed into the network but can be consumed locally and the grid does not suffer too high load peaks.

The EV simulation was executed with a different MATLAB® model created by Lindgren [37]. Lindgren model is based also on nodes, but they are a bit different by nature from the nodes of this thesis. They are smaller and in practice one workplace, shopping centre, hobby place or block of flats forms one node. The nodes are connected to each other by roads. Each car in the simulation has its own home and workplace. Cars move in the city between the nodes and consume electricity from their batteries, and when they arrive at a node with charging sockets, they are able to recharge. The model is described more thoroughly in Lindgren's master's thesis.

The connection between the two models was made by dividing the nodes of this thesis into four subnodes for the Lindgren model, one node is empty, one for houses, one for

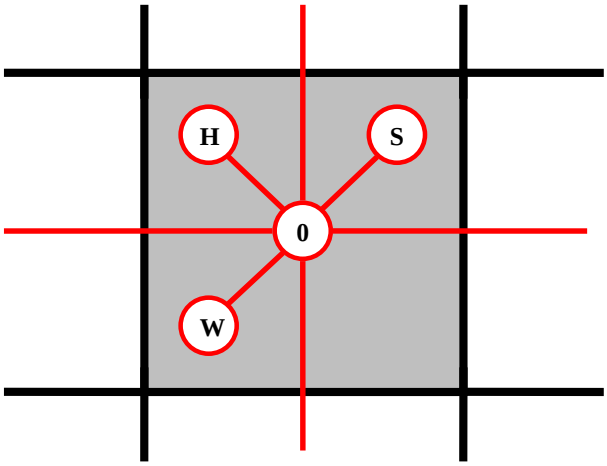

Figure 3.3: The connection between the nodes of this thesis and Lindgren's EV simulator. The node of this thesis (grey square) is divided into four subnodes: empty node (0), home node (H), workplace node (W) and node for shops, hobbies etc. (S).

workplaces and one for other purposes (shops, hobbies, etc.). Schematic illustration of this is in Figure 3.3. The empty nodes are used to connect the nodes of this thesis to each other in the Lindgren model. Distances of the subnodes from the empty central node are half of the width of the square node of this thesis. This distance is significant because it affects directly the kilometres driven by the cars.

The urban structure of the city (explained earlier in Section 3.1.3) is included to Lindgren model with the car data. More cars could be chosen to be those that have their home nodes where the household density is larger. Respectively, the work places of the cars are chosen in a way that the majority of the cars has their workplace in areas with high office or manufacturing density. The shares of which car lives where and where its working place is, are directly proportional to the consumer type densities of Equation 3.1.

3.5.1 Smart charging strategy

The goal with EVs was to cut off the highest local production peaks of electricity. In other words, the EVs were wanted to charge at the time when PV cells are producing too much electricity for the network to transport.

It was not possible to run both MATLAB models simultaneously so that they would have communicated or interacted with each other. Instead, the simulation was run so that first the model of this thesis was run through without any EV impact. Large PV installations were expected to cause heavy overflows in the electrical grid. After this first simulation was run, the overflow moments were tracked for every node at every time step. At the same

time it was found out how much the solar production should have been reduced, so that the overflows would not have occurred. This way so called *must-profile* was created for every node. It tells how much the cars at the node must recharge their batteries at each time step i.e. how much they have to increase the consumption so that the high production peaks do not have to be exported to the grid.

It might also be possible that the cars would be recharging too much. For example if there is no solar production but the cars need huge amount of energy, they might cause the overflows to the opposite direction to PV overflows. Because of this, also another profile was tracked with the must-profile. This one is called *may-profile*. It tells how much the vehicles are allowed to charge.

Based on these two profiles, a charging strategy for the cars was created. The most important feature of a smart strategy is that it has to be at least somewhat predictive. All smartness and optimization possibilities will be lost if the strategy does not know anything about the future. It would not be possible to maintain the storage or charging capacity (i.e. the deficit in batteries) for the moments they would be needed.

The strategy used here assumes that the must- and may-profiles as well as the traffic (i.e. locations) of the cars are known two days beforehand. The algorithm tracks the must-profile and detects if the profile differs from zero. In other words, the algorithm finds when and how much local EV charging is needed. After this, it finds out which cars are at the node in question at those time steps. It is good to notice that the cars may move to the node later and be now somewhere else. Because the algorithm knows the traffic of the cars, it knows also how much energy they are using from their batteries before reaching the node and before the critical time steps. Based on these pieces of information (how much recharging is needed, which cars are at the node at the must-recharge moments & how empty their batteries need to be then) it is possible to tell the car if it may or must not recharge now. May-profile is taken into account by just checking that the recharging power does not exceed the value in the profile. If it does, the power could be reduced so that the problem will be solved.

Chapter 4

Energy profiles and case studies for Helsinki and Shanghai

This chapter describes the present energy infrastructure in Helsinki and Shanghai. Consumption and production profiles are represented. Since direct hourly data of the consumption profiles was not available, the chapter describes how the hourly load profiles were created based on the available data. Finally, the chapter tells what types of renewable energy scenarios for the cities are simulated with the model. The results are represented in the next two chapters.

4.1 Helsinki

Helsinki is a northern city (60°N) with about 590 000 inhabitants. The population of the whole metropolitan region is over 1.3 million. Helsinki is fairly sparsely populated which has its influences on the energy infrastructure. The population density is only 2800/km^2 (450/km^2 in metropolitan region).

The climate in Helsinki has very large seasonal variations which affect the energy consumption a lot. The temperature may vary from -30 °C at winter to over $+30$ °C at summer. The amount of daylight varies too. At winter, the light time is very short (only about 5 $\frac{1}{2}$ hours of daylight during the winter solstice), and at midsummer, the sun shines over 18 hours a day. This has a direct impact on the lighting needs, and thus on the electricity consumption.

Only electricity and heat are considered in Helsinki cases. The cooling load (1 TWh) throughout the year is so small compared to electricity and heating demands that it is neglected here. Data from year 2006 was used in the simulations. The yearly electricity demand in Helsinki was 4.37 TWh and the heating demand 6.60 TWh. [38]

Traditionally in Helsinki, electricity and heat are produced in large centralized power plants that use mainly natural gas and coal as their fuel. The plants are combined heat and power (CHP) plants that can produce both electricity and heat with an overall efficiency of about 80 %. Because of the combined production, there is more electricity produced than consumed in Helsinki. In 2006, altogether 6.31 TWh of electricity was produced in the city, and the share of CHP production was 4.93 TWh [39]. In practice, all this Helsinki-produced energy originates from fossil fuels. In other words, Helsinki produces much more fossil electricity than it needs itself.

The heat is produced mainly with CHP plants but during the cold days at winter additional production is needed. For this purpose, there are ten pure heating plants in the city. Seven of them use oil as their fuel and three of them natural gas. Similarly to electricity, also heat is thus produced almost in its entirety by fossil fuels. Delivering the produced heat to the customers, there is an extensive district heating network in Helsinki. It is wide and covers practically the whole city. 93 % of the heat load of the city is met by district heating [40]. Thus, there is an existing infrastructure to transport not only electricity but also heat energy everywhere in the city.

4.1.1 Electricity consumption profile

Because no hourly data were available, the consumption profiles had to be made with the help of the available information. The electricity profile is characterized by daily, weekly and annual rhythms. The consumption is much higher at daytime than at nights, and at weekends, it drops significantly. At summer it is smaller than at winter.

The profile (consumption for every hour of the year) is based on two graphs (not numerical data) acquired from energy company Helsingin Energia and the consumption data of the whole Finland in 2006 (available in numerical form in [41]). Helsingin Energia graphs showed the electricity consumption of Helsinki in 2010 throughout the year and one typical load of one week.

The starting point was to fit a cosine curve to the national data. After the wave length was fixed as one year, the cosine curve is defined by its amplitude, average and phase angle. The phase angle (i.e. the moment of the maximum consumption) was taken directly from the national data fit. It is logical to assume that the maximum occurs approximately at the same time in Helsinki and in whole Finland. The maximum of the cosine was found to be on 20th of January.

The average (constant term) of the consumption was calculated by dividing the overall consumption of 4.37 TWh with 8760 (number of hours in a year). It was thus 499 MW. The last free parameter, amplitude, was estimated based on the yearly graph from Helsingin Energia. It was chosen to be 100 MW.

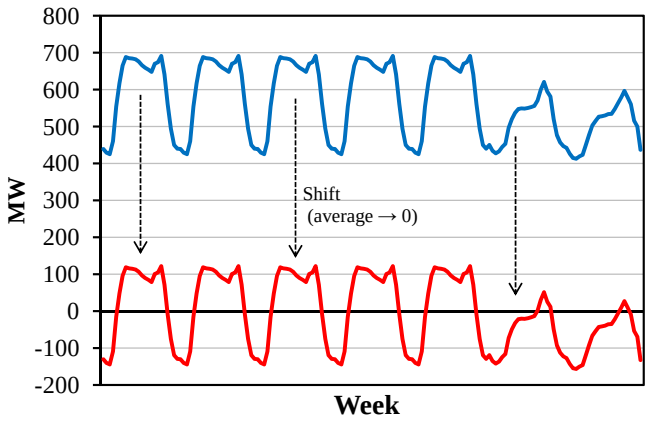

Figure 4.1: Typical week profile and how it is shifted so that the average is zero.

The cosine tells only the yearly variations. Daily and weekly profiles had to be added still. This was done with the help of the weekly profile of Helsingin Energia. The numerical values of one weekday, Saturday and Sunday were extracted from the graph, and then combined as one-week profile (blue curve in Figure 4.1). The values were shifted so that the average of the week became zero (red curve). The weekly and daily variations were added to the profile by just summing the shifted week profile (extended to all weeks of the year) and the annual cosine curve together.

On top of the seasonal variations, momentary perturbations like extreme weather conditions or national holidays were added to the profile. They were taken into account by calculating the moving weekly average of the national data which was then compared to the national cosine fit. It was found out how much the average differs from the cosine relatively. The same relative variations were then added to the Helsinki profile. The variations were scaled by factor 0.7 so that they were not as striking as on national profile.

The final electricity consumption profile for the city is shown in figure 4.2. The red curve is the cosine curve on which the daily, weekly and other temporal variations were added.

4.1.2 Heat consumption profile

The heat consumption profile is based on the hourly temperature data of Helsinki Kaisaniemi meteorological observation station. The data was acquired from the Finnish Meteorological Institute. The outside temperature is by far the most important factor modifying the heating demands. The other factor that is considered here are the daily routines of people. At winters, the heating demand is bigger at nights when the sun does not shine and the temperature is lower. The difference between day and night consumption is however a bit less than what one could think on the grounds of temperatures. This is caused by domestic hot water use

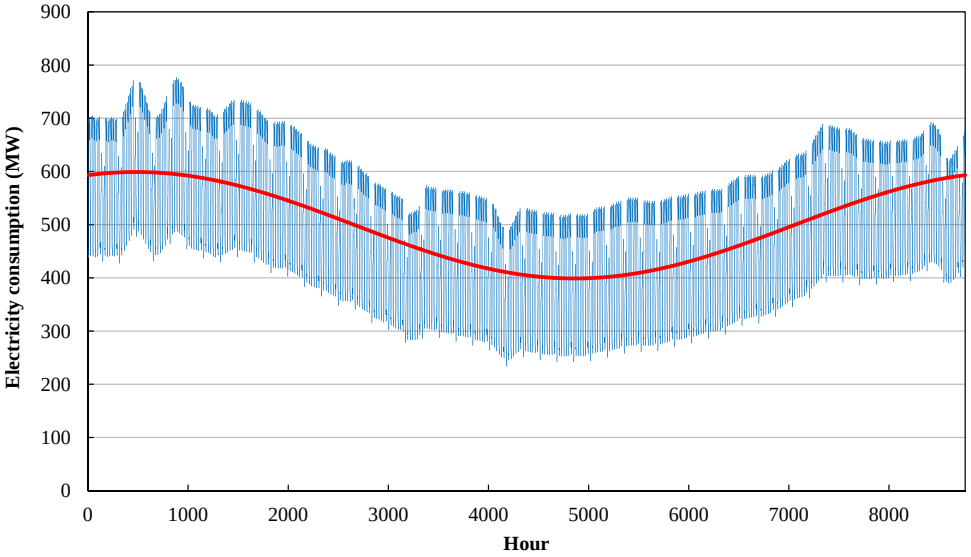

Figure 4.2: Electricity consumption profile in Helsinki and the cosine curve on which it is built.

that is in practice zero at night time. For the same reason, the heat consumption at summers is higher at daytime than at nights.

The first approximation is that the heat flow through the walls (lost heat) is directly proportional to the temperature difference between the outside air and the inside of the house. The temperature-dependent heating demand behaves similarly. The domestic hot water use is assumed to be independent of the outside temperature. These assumptions lead to a curve like the one in Figure 4.3(a). There is a decreasing linear part when the temperatures are cold, and after the temperature rises above a certain limit, no space heating is needed and the function becomes constant that describes the domestic hot water use.

The curve does not take the daily variations into account. This is done with the profile in the adjacent Figure 4.3(b) that presents the daily variation caused mainly by the hot water use. The data for the daily profile was extracted from the example graph of one typical day in Helsinki. The graph was acquired from Helsingin Energia. This daily profile is copied for every day of a year and then summed together with the profile formed on the grounds of the temperature data and Figure 4.3(a).

Helsingin Energia offered same kind of annual graph of the heat consumption than it did with electricity. The temperature–heating demand curve (Fig. 4.3(a)) is defined by its slope, the turning point and the constant. Based on the real annual graph these three parameters were fitted. The fitting was made after the daily variations were added on. Based on the real graph, the minimum of the heat consumption should be about 170 MW and the maximum peaks a bit more than 2500 MW. The strictest boundary condition was

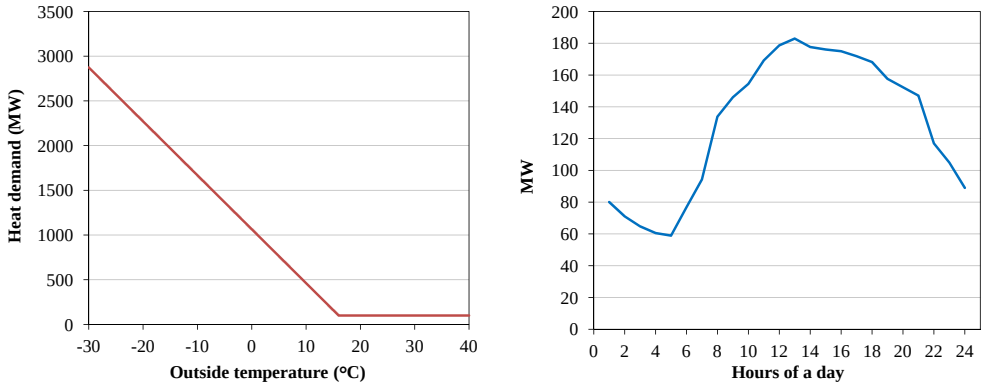

(a) Heat demand as a function of outside temperature.

(b) Daily variation in heat load.

Figure 4.3: Background data for creating the heat load profile.

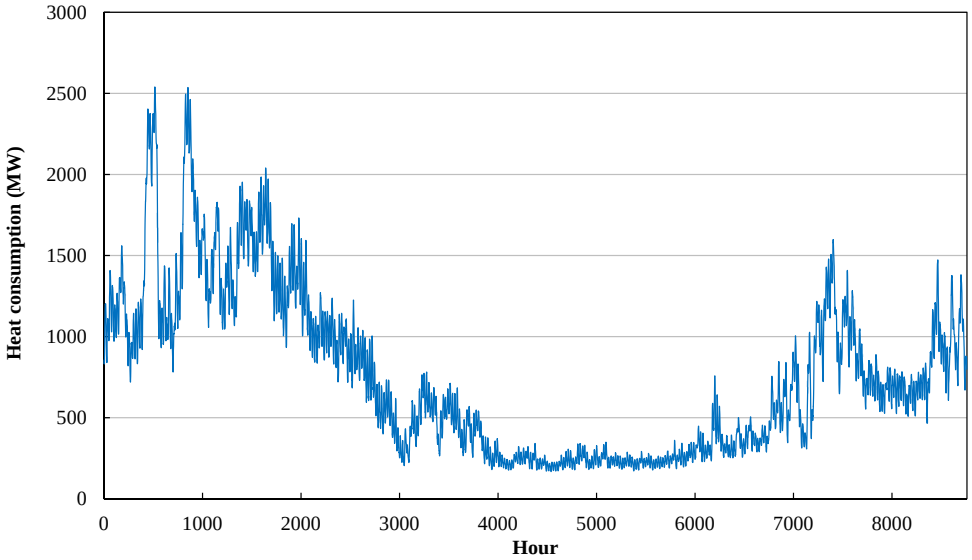

Figure 4.4: Heat consumption profile in Helsinki.

that the total consumption should match with 6.60 TWh. By fitting the parameters, the profile in Figure 4.4 was created.

4.1.3 City model and the node-wise profiles

The land area of Helsinki is 213.75 km^2. If sparsely populated islands and wooded areas are excluded (e.g. the new very sparsely built Östersundom area covers over 30 km^2), the area is close enough to 100 km^2 so that the city can be modelled with 10 km $\times$ 10 km grid. The grid of this size and one hundred 1 km^2 nodes was used for Helsinki.

Table 4.1: Parameters to define the consumer type densities.

Parameter	$d_{0,i}$ (MW/km^2)	α_i (1/km^2)	$r_{0,i}$ (km)
Office	4.167	0.06	0
Manufacturing	0.833	0.02	12
Households	0.565	0.006	3

The electricity and district heating networks were made with the method that connects the node to the second closest node from the base node (see Section 3.1.1). The city center was located at the point (3 km, 3 km) so that it is in the south-west corner of the city. The electricity and heat networks are represented in Figure 4.6.

The consumption profiles (Figures 4.2 and 4.4) were divided among the nodes according to Section 3.1.3. The parameters of the Gaussian densities in Equation 3.1 are represented in Table 4.1. The densities are given as megawatts of electricity per square kilometer, which means that the temporal base profiles h_i in Equation 3.2 are dimensionless. They just tell *relatively* how the consumption behaves during a day. The densities were made mainly according to electricity but they were used with the heat profiles as well. The absolute value of the densities are not exactly what it will be in the final node-wise profiles, because Equation 3.4 scales the values finally so that the sum of the node-wise heat consumption values match with the real heating demand of the city. The consumer type-wise energy densities d_i are shown in Figure 4.5(a) and the temporal base profiles h_i for electricity in Figure 4.5(b). The base profiles were scaled so that the average of each of them equals one.

Figure 4.6 shows how the total consumptions (Figure 4.2 and 4.4) are divided among the nodes. The same figure shows also how the consumption is concentrated in the city

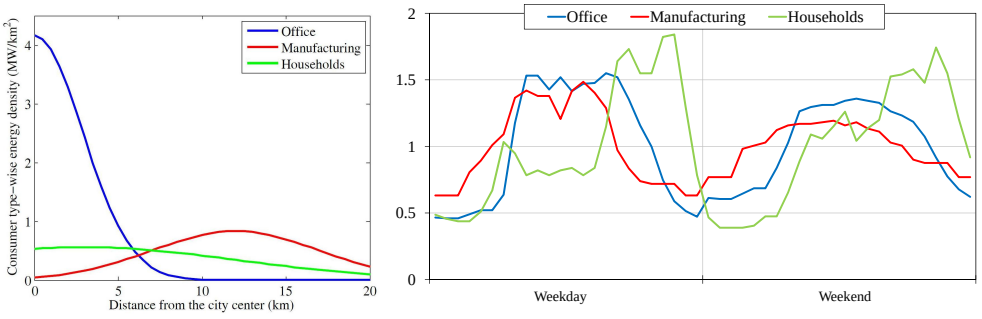

(a) Densities of different consumer types as a function of the distance from the city center.

(b) Temporal relative base consumptions of electricity.

Figure 4.5: Background data for dividing the consumption among the nodes.

center area. The average consumption in the center is about 2–3 times higher than on the outskirts (for electricity, 7–8 MW/km^2 and 3–4 MW/km^2 respectively). The annual variation in heating is much stronger than in electricity. The maximum electrical peak load is approximately 3 times higher than the minimum load. The same ratio for heat is about 13. The difference shows clearly in figures 4.2 and 4.4.

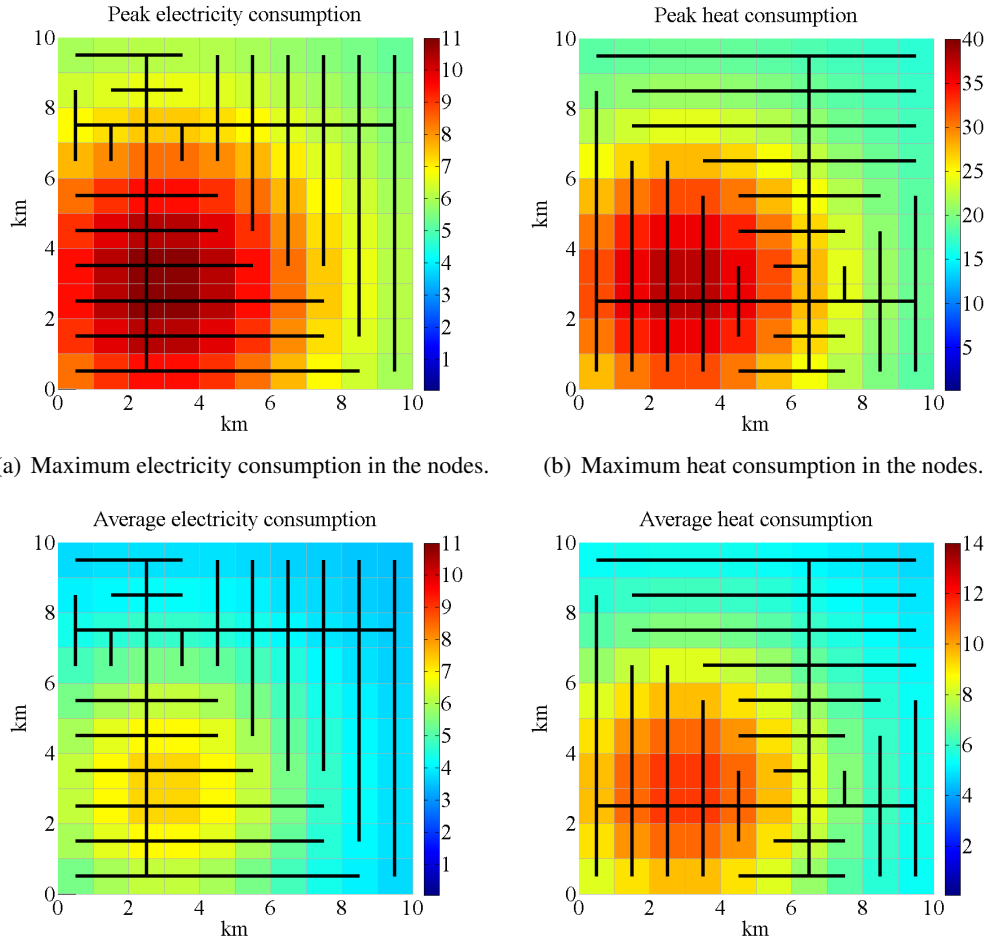

(a) Maximum electricity consumption in the nodes.

(b) Maximum heat consumption in the nodes.

(c) Average electricity consumption in the nodes.

(d) Average heat consumption in the nodes.

Figure 4.6: Maximum and average consumptions of the nodes in Helsinki case. Spatial resolution is 1 km $\times$ 1 km and power densities are given as MW/km^2. Energy networks are shown by black lines. One should notice that the color scales in heat graphs (right-hand side) are not same.

4.1.4 Case studies

Reference case. In the Helsinki reference case, no production is located within the grid area. Thus all electricity and heat are imported from the base node. In other words, one node takes care of the whole consumption of one energy type. This imitates the situation where the energy is produced at large centralized power plants.

Large scale wind power. In the first renewable energy case, there was a large scale (hundreds of megawatts) offshore wind farm was located on the sea area south from the city. The annual wind production profile is represented in Figure 4.7. The four-week moving average curve in the figure shows that the turbines produce more electricity at winter than at summer. Because of this, there is a small positive correlation between the energy consumption and wind production, although wind production is very intermittent.

The purpose is to investigate how much wind power could be installed in the system so that no overflows occur (comparison with the reference case). The location of the wind power connection affects a lot to the amount of potential wind capacity, which why different locations in the grid are tested. It is studied how much the capacity could be increased if the production that exceeds the flow channels is converted into heat (by electric resistance or heat pumps) and then fed into the heating network.

Solar cells and electric vehicles. In practice, wind power at least in large scales is centralized production. Solar energy however is not. It can be integrated quite easily into the urban structure. For example roofs offer lots of free and sunny space to be utilized

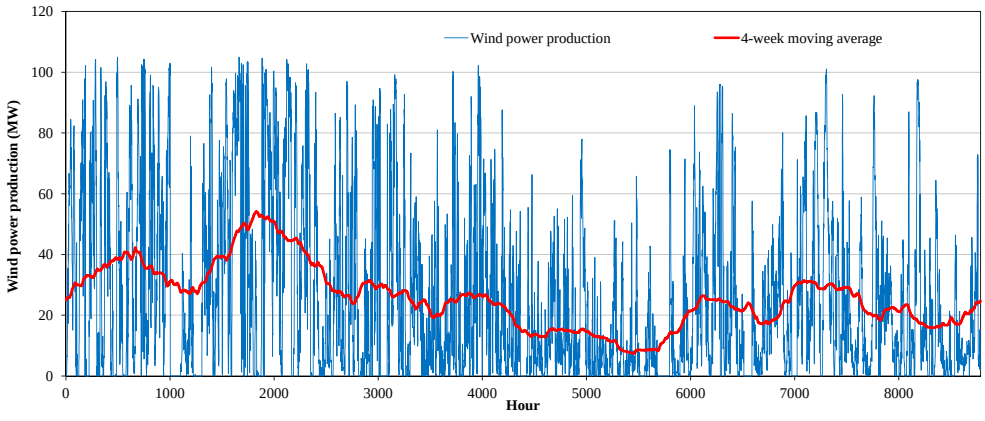

Figure 4.7: Electricity production curve of 100 MWp wind power park and its four-week moving average.

in solar energy production. In opposite to wind power, solar energy production is strongly concentrated in the summer time. This shows clearly in Figure 4.8.

Network-wise, the PV cells should be installed according to the consumption, i.e. more cells in the high-consumption areas. This would minimize the spatial transportation needs. However, the problem may be that the physical area is limited. If the city center has not enough free space for the cells, they have to be located outskirts of the city which can then cause overflows in the grid. The location of the cells and the overflows are studied.

Plug-in electric vehicles may be one solution to the overflow problem. Smart recharging of them could transform the energy balances conveniently. This is option also investigated.

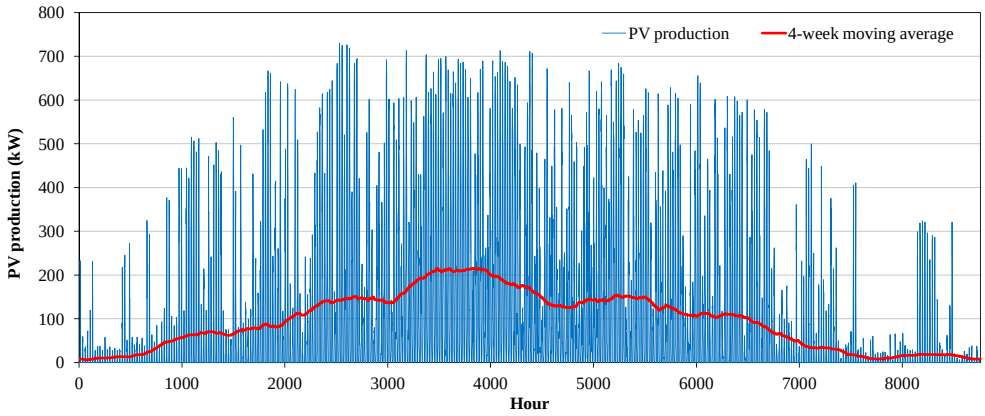

Figure 4.8: Electricity production curve of 1 MWp photovoltaic cell installation and its four-week moving average.

4.2 Shanghai

Shanghai differs greatly from Helsinki in many ways. Shanghai is a southern (31°N) megacity with population over 23 millions. The most densely populated districts have populations over 40,000/km^2. Such huge amounts of people require a lot from the energy system.

In Helsinki, the total energy consumption consisted of electricity and heat (fossil fuel traffic is not considered in the thesis) and cooling load was assumed to be so small that it could be dismissed. In Shanghai however, the situation is completely different. The summers are so hot that the cooling of the buildings forms an essential part of the energy consumption.

Data from year 2004 was used as input for the model. The electricity consumption was 82.1 TWh. Detailed data on the heat and cooling consumption was not available except some maximum values [42].

4.2.1 Electricity consumption profile

The hourly electricity consumption profile of Shanghai is based on data extracted from two graphs. The first of them tells the monthly peak and off-peak values of electricity consumption [42] and the second one describes the daily variation in electricity consumption [43]. The rough hourly data for the whole year was got from the monthly data of peak and off-peak consumption by spline interpolation. This produced hourly upper and lower limits of the consumption (Figure 4.9(a)). The daily variation curve (Figure 4.9(b)) was then used to get the final profile. For each hour, the final consumption between the peak and off-peak curves was chosen in relation to the daily variation curve. This means that every day the consumption of the 10th hour (the hour with maximum value at daily variation curve) was designated to be the value at peak curve in Fig. 4.9(a). Respectively, the fourth hour of a day got its consumption value from the off-peak curve.

The final consumption profile is shown in Figure 4.10 with light green line. 82.0 % of cooling and 43.7 % of heating load are satisfied with electrical chillers and heaters [42]. Their share is included in the green curve. In the model however, different energy types must have their own consumption profiles. Because of this, there is another graph in the same figure (blue curve) that shows the pure electricity consumption i.e. the one from which the load caused by heating and cooling has been reduced. How the heating and cooling loads were created, is represented in the next section. The annual consumption of electricity

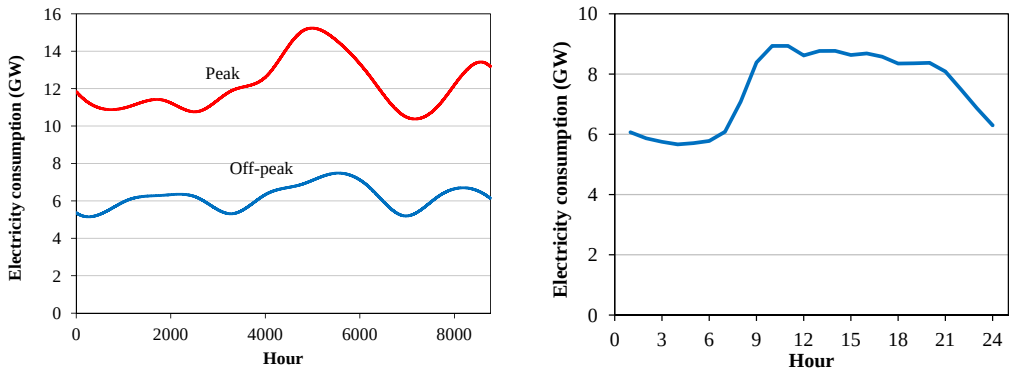

(a) Spline interpolation of monthly peak and off-peak consumption.

(b) Daily variation.

Figure 4.9: Background data for Shanghai electricity consumption.

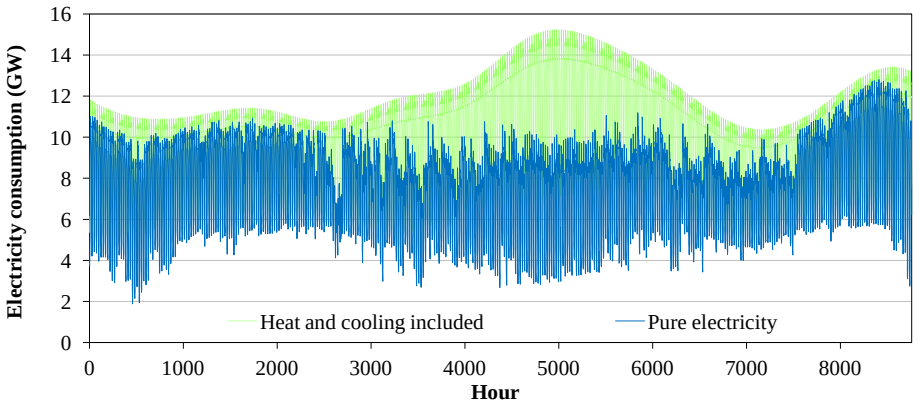

Figure 4.10: Electricity consumption profile of Shanghai. The blue line is the consumption without the electricity used in heating and cooling purposes. The green line takes also heating and cooling electricity into account.

without heating and cooling is about 65 TWh.

4.2.2 Heating and cooling load profiles

The heat and cooling profiles that were created for the simulations are based on the temperature data from Shanghai in 2004 [44]. The data consisted of the highest and lowest temperatures of each day. It was assumed that the highest temperature during a day is achieved at 2 pm and the lowest one at 3 am. This produced two data points for each day, and the spline interpolation was used to get hourly values.

The hourly temperature data was turned into heating and cooling loads. For this purpose a graph from [45] was used. The data is represented in Figure 4.11. The graph shows the energy performance of earth-to-air heat exchangers as a function of ambient temperature. It is a good approximation for relative heating and cooling loads with regard to the temperature data. The original heating graph (red curve) in [45] decreased to zero at higher temperatures, but in order to take the domestic hot water use also at summers into account, the graph was raised so that it levels out as a positive constant at higher temperatures.

Figure 4.11 was applied to create the preliminary heating and cooling load profiles which were scaled so that the overall heating and cooling consumptions matched with the reference values. 82 % of cooling in Shanghai is done by electrical devices [42]. In 2004, the peak electric load of air-conditioning in Shanghai was 6,860 MW [46]. It was assumed that this cooling load was satisfied by heat pumps with COP $= 3$. These numbers state that the maximum peak of all cooling energy demand is $3 \times \frac{1}{0.82} \times 6{,}860$ MW $= 25{,}860$ MW.

In [47], it is represented that the cooling load is approximately two times bigger than the heating load in Shanghai (66.27 kWh/m^2 and 36.95 kWh/m^2 respectively). Based on

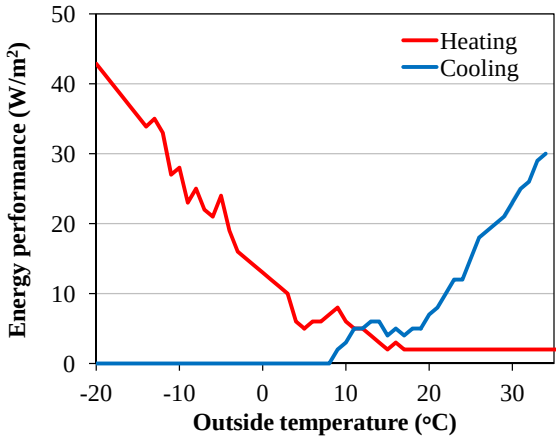

Figure 4.11: Specific energy performance of earth-to-air heat exchangers as a function of ambient temperature [45].

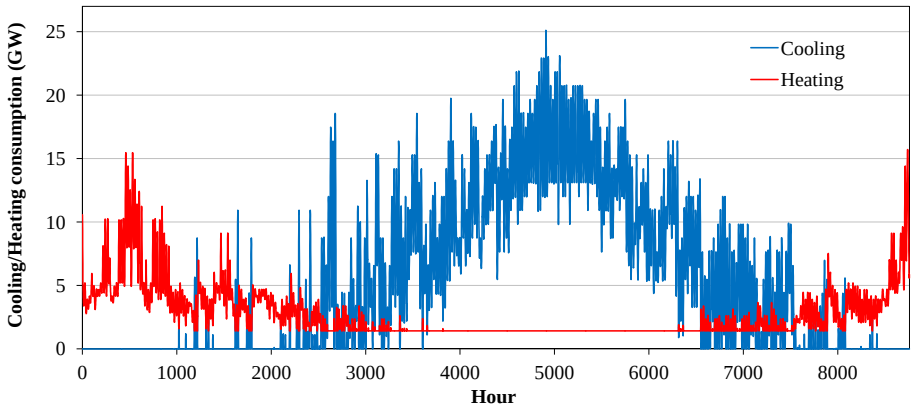

Figure 4.12: Cooling and heating consumption profiles in Shanghai.

this, the heating profile was scaled so that the annual heating energy consumption is about half of the cooling consumption. The final profiles can be seen in Figure 4.12. The overall cooling consumption of the year is 47 TWh and heating consumption 24 TWh.

4.2.3 City model and node-wise profiles

The area of the municipal Shanghai is over 6 000 km^2. The majority of the population is concentrated strongly on a much smaller area. The outskirts of the city have population density of only a few hundred people per square kilometer. In downtown, the number can rise up to 50,000.

Shanghai was modelled with a 50 km $\times$ 50 km grid with one hundred nodes. The grid covers most of the city area. The city center lies in the north-east part of the municipality,

and in the model, it was put to coordinate point 42.5 km, 42.5 km.

Population and energy consumption are strongly peaked at the city center. For this reason, a 25 km^2 node was too large to describe accurately the situation in the central parts of the city. Therefore, the city center node was divided into one hundred sub-nodes.

The energy networks were created with the same method as in Helsinki. Every node was connected to the second closest node from the city center. In Shanghai four different energy types were examined (electricity, heat, cooling and gas) but only two of them (electricity and gas) were assumed to have a network. In spite of this, a network was created for all of them as the model requires but heating and cooling networks were never used. The gas network is shown in Figure 4.13. The electrical network is shown with energy consumption distributions in Figures 4.15–4.16.

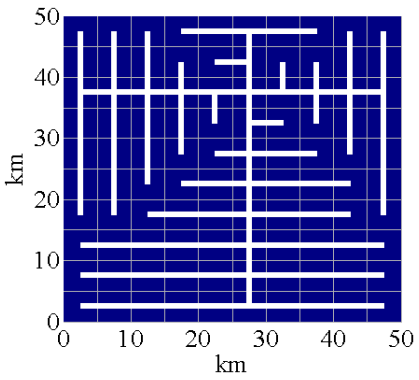

Figure 4.13: Shanghai gas network.

Distributing the overall consumptions to the nodes was carried out in the same way as in Helsinki. The parameters of the consumer type densities d_i (Equation 3.1) are in Table 4.2. To get the household density to extend to the whole city, a constant term was added to the original equation. Figure 4.14 shows the relative densities of the consumer types as a function of the distance from the city center.

The same temporal base profiles h_i (in Equation 3.2) were used as in the Helsinki case. They can be seen in Figure 4.5(b). A fraction of randomness was added to the nodal con-

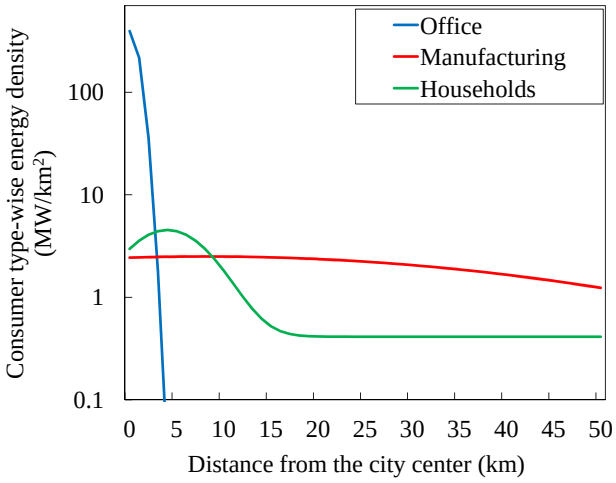

Figure 4.14: Consumer type densities as a function of the distance from the city center.

Table 4.2: Parameters to define the consumer type densities.

Parameter	$d_{0,i}$ (MW/km^2)	α_i (1/km^2)	$r_{0,i}$ (km)	constant (MW/km^2)
Office	395.8	0.6	0	–
Manufacturing	2.5	0.0004	8	–
Households	4.1	0.03	4	0.6

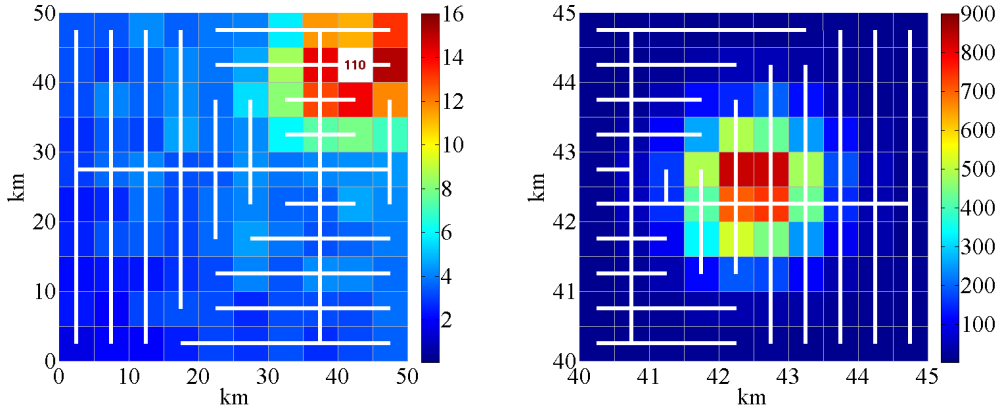

(a) Peak electricity consumption (whole area).

(b) Peak electricity consumption (city center).

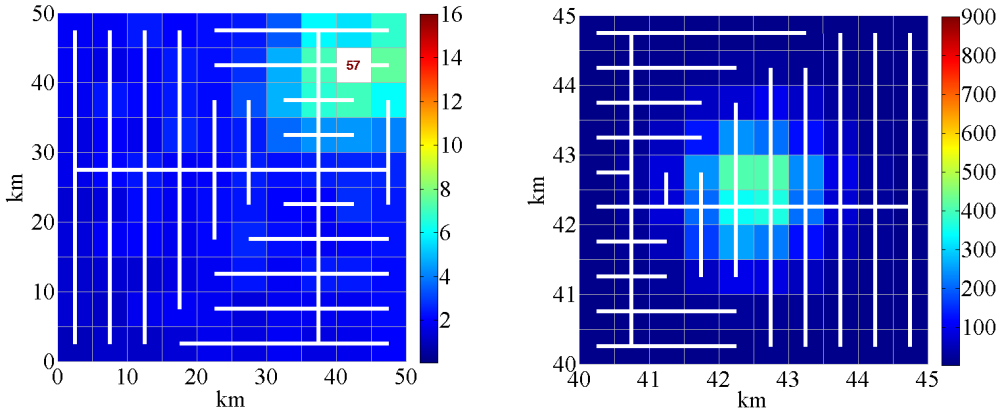

(c) Average electricity consumption (whole area).

(d) Average electricity consumption (city center).

Figure 4.15: Peak and average electricity consumptions of the nodes in the Shanghai case. Power densities are given as MW/km^2. The left graphs show the consumption in the whole metropolitan Shanghai and the right graphs in the most central node (the white node on the left that does not fit to the color scale). The electrical networks are shown by white lines.

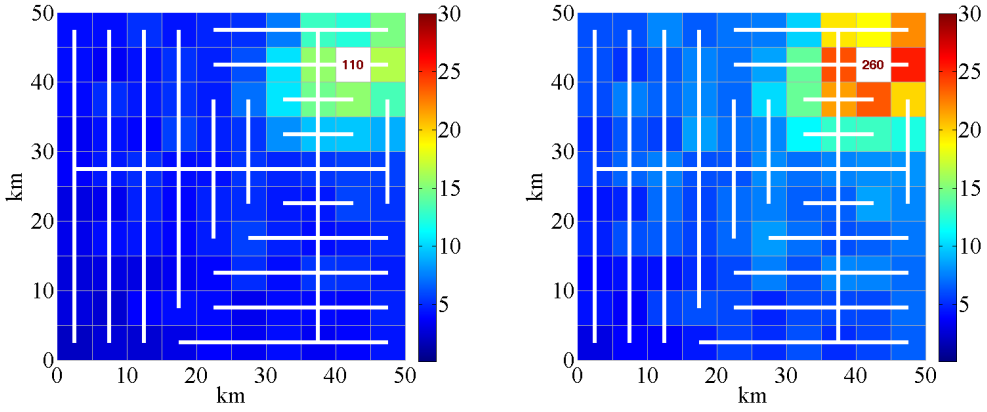

(a) Peak heating consumption (whole area).

(b) Peak cooling consumption (whole area).

Figure 4.16: Peak heating (left) and cooling (right) consumptions of the nodes in Shanghai case. Power densities are given as MW/km^2. The values of city center does not fit into the color scale and is thus given as number. The electrical network is shown by white lines.

sumption profiles. This was not made in Helsinki case, but since now there are many same type of nodes (with relatively small energy demand in the outskirts), some variation between them was wanted. A random number between 0.8 and 1.2 was chosen for every node and the nodal profile was multiplied with this factor.

The final node-wise distribution of energy consumption is visualized in Figure 4.15 for electricity and in Figure 4.16 for heating and cooling. The figures show also the electrical network.

4.2.4 Case studies

Reference case. 43.7 % of heating and 82.0 % of cooling demand are met by electrical heaters, heat pumps or radiators (see Section 4.2.1). Natural gas is another energy source for heating and cooling. It covers 7.8 % of heating and 4.0 % of cooling energy [42]. In the reference case, the electricity is produced in large power plants outside the city, and in the model all electricity is imported from the base node. It is assumed that all electricity-made cooling is done with heat pumps with COP = 3. For heating purposes also electric resistance (COP = 1) can be used which why the COP for heating is assumed to be about 2 in the model. When converting gas into heat, the COP is set to 1 and for cooling to 0.7. For example, simple absorption chillers work approximately with COP = 0.7 [48]. The rest heating and cooling are done with oil and coal. In the model, this energy is taken from the (virtual) heating/cooling network and its base node.

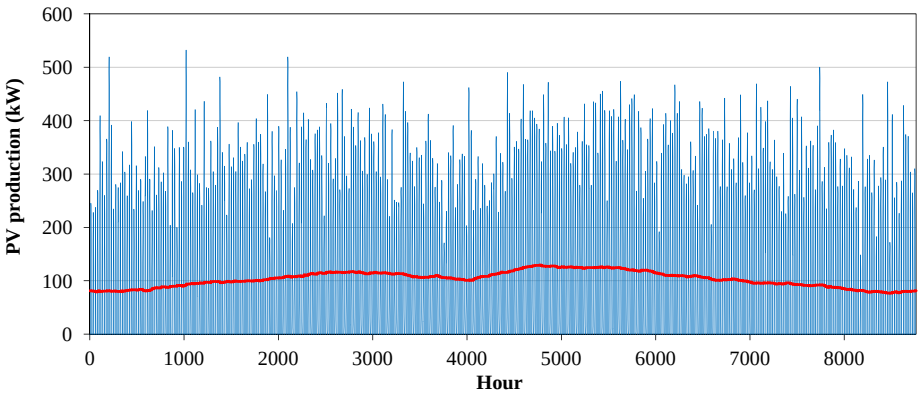

Figure 4.17: Electricity production curve of 1 MWp photovoltaic cell installation and its four-week moving average (red curve) in Shanghai.

Large-scale photovoltaics. First renewable energy case in Shanghai discusses large-scale PV panel installations. Significant shares of PV power are investigated. In the first case, despite the huge electrical load, the city achieves the situation where momentarily all consumed electricity is produced by PVs. In addition, a case is studied where a little overproduction is allowed (at some moments the production may exceed the consumption).

A PV production curve for Shanghai is represented in Figure 4.17. When comparing it with the same graph for Helsinki (Figure 4.8), one can see that it is much more evenly distributed throughout the year, and that also the peak power is not as high. Main reason for the lower peak production is that the temperatures of the panels remain cooler in Helsinki and thus higher efficiencies can be achieved.

The intention is to find out how large shares of the overall consumption can be met by PVs and the magnitude of the overflows that the PV panels cause. Presumably, overflows will occur at some point when adding more and more PV panels. Another way to study this is to find out where does the energy that is consumed in the central city, come from (i.e. how much the outskirts feed the city center).

Trigeneration in the city center. One way to reduce the overflows caused by the heavy PV installations in the outskirts of the city is to replace some of the outskirt PV capacity with small-scale trigeneration plants in the city center. The consumption peaks in the center area are so high that in any case it could be impossible there to install enough PV panels to cover the whole demand.

It was investigated that if the overflows are born, how much PVs have to be removed from the overflow nodes. The removed production capacity was replaced with fuel

cell based trigeneration in the center. The fuel cells use natural gas to produce electricity with efficiency 0.4 and heat with efficiency 0.4. Cooling is achieved from heat by absorption chillers working with COP = 0.7.

On top of this avoid-overflows type of approach, another approach was studied. In this case, the self-use limit of electricity should not be broken. This means that at maximum, the distributed production can match with the consumption, but no energy is exported outside the city. The question to be answered is that how much PV panels it is possible to install if certain percentage of the heating and cooling demand is covered with trigeneration. In other words, the fuel cell in the city center produces a fixed share of the thermal energy consumption at each hour. At the same time the cell produces electricity (the amount is determined directly by heating and cooling demands). This electricity production affects the available PV capacity.

Finally, it is studied (on top of the overflow reductions) how the trigeneration affects the shares of DEGS produced energy. Because rather same studies were made for both the pure PV case and the PV case with trigeneration, the results could be compared mutually.

Chapter 5

Helsinki case study

5.1 Reference case

The simulations in Helsinki were started with the reference case where all energy is imported from the base nodes. The reference case is needed before any analysis of the renewable energy cases can be done because it defines the flow channels (equation 3.19) that are represented in Figure 5.1. The figure shows two strong trunk lines starting from the base node and many smaller lines branching out of them.

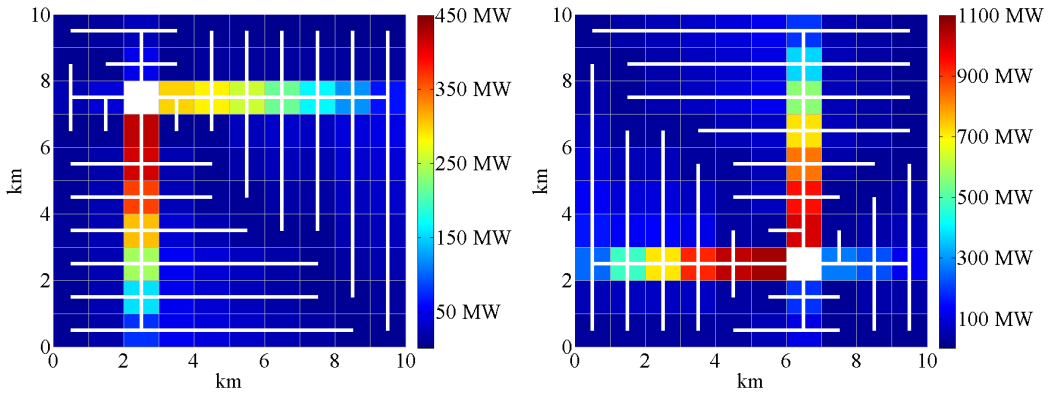

(a) Electricity.

(b) Heat.

Figure 5.1: Flow channels in Helsinki case. The colour of the node represents the channel of the line pointing from the node towards the base node (white nodes). Energy networks are shown by white lines.

5.2 Large scale wind energy case

The first renewable energy case in Helsinki was the one with a large scale offshore wind farm connected to the energy system. The purpose is to find out how much wind energy it is possible to fit in the system and how much it can be increased if part of the wind-produced electricity is converted to heat.

The farm is assumed to be located at the sea area south of Helsinki. Since constructing heavy high-voltage lines deep inside the city can be very limited in urban environment, the first guess for the connection point is next to the sea at the end of the other electrical trunk line. This is the node at coordinates 2.5 km, 0.5 km, marked with letter A in Figure 5.2.

The geographical location close to sea is one advantage of the point A. Because the location is at the very end of the heat network, the heat conversion possibilities are there rather scarce (the network is weak). In this sense, much better place is the node marked with B at coordinates 2.5 km, 2.5 km. The node lies along the main lines of both networks and also the electrical network is stronger than at node A (see Figure 5.1).

Same type of a “sweet spot” (along trunk lines in two networks) as B can also be found in the node marked with letter C. Point C is not anymore close to the wind farm, but as it is presumable that it will increase the wind power capacity drastically it is taken under investigation. With respect to both networks, point C lies on the other side of the base node than point B, which why that they do not affect or disturb each other in any way.

Figure 5.3 shows an example how the wind power connection affects the flows in the network. The figure represents the case where wind power connection is made to the point B (node 23, wind turbine icon). The horizontal axis represents the other main line in electrical network (node numbers 21–28, highlighted in the small network picture in Fig. 5.3), and

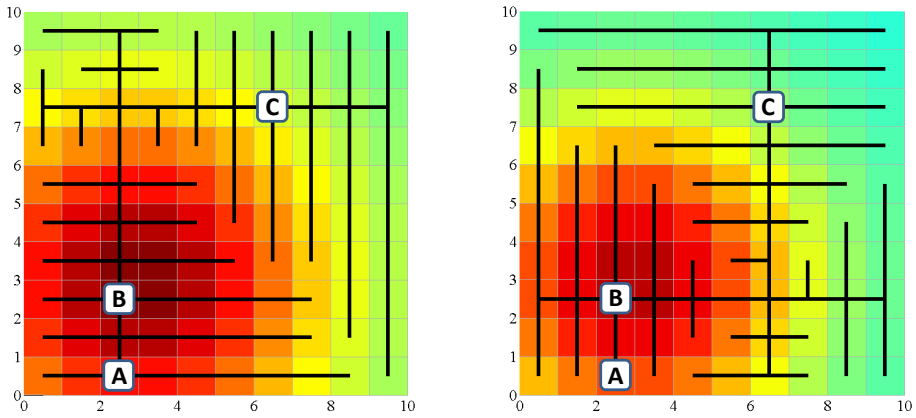

Figure 5.2: Options for the location of wind power connection, left: electrical network, right: heating network.

on the vertical axis, there are the amounts of flowing electricity.

The pink and light blue areas in the background are the flow channels for each single section of the whole line. Thus one can see that the flow channels are larger near the base node (node 28, right end of the horizontal axis). Positive values mean that the electricity is flowing downstream (away from the base node) and respectively negative values upstream (towards the base node). The curves in the plot show the minimum flows over the year with different amounts of installed wind power. The *minimum* here means the maximum amount of electricity that is flowing towards the base node. In practice this happens at some time step when wind production is high and consumption low.

The reference case with no distributed production at all stays always on the positive side, meaning that electricity is never flowing towards the base node. The more the amount of wind production increases the more electricity is also flowing upstream (negative flows). Another point is that adding wind production to a certain node, has no effect on the flows at the tail side of the grid (below the wind connection point).

All in all, when the curve of the case stays inside the flow channels, overflows do not occur. But if the wind park is too large (two lowest curves), the electricity transportation becomes too huge. This creates overflows, and the grid is put under an additional stress compared to the reference case.

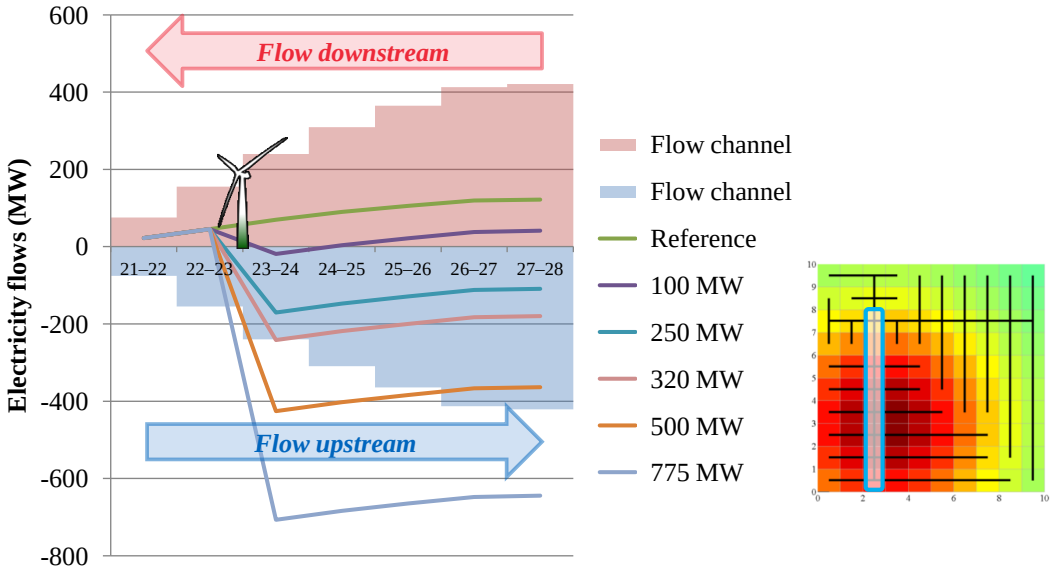

Figure 5.3: The effect of wind power on the main electrical line. Wind power production is connected to node 23 (= point B, wind turbine icon). Curves show the minimum flows over the year (i.e. the greatest flow towards the base node). The light coloured area represents the flow channels. The line in question is highlighted in the small network picture.

The conclusion from Figure 5.3 is that point B has capacity for 320 MW of wind power. Larger wind farms would cause overflows in the grid. This type of investigation was done to all three nodes (A, B and C), and the results are gathered to Table 5.1. The table includes the results also from the cases where electricity is converted to heat (COP = 3 or COP = 1) and sent to the heating network. COP of 1 means in practice that the electricity-to-heat conversion is done directly by electric resistance. COP of 3 represents heat pumps. The conversion was located either at the node of the wind power connection alone or there and at the downstream nodes of it. Upstream conversion is not possible because the upstream flow channel is already full.

The table shows how much the location in the electrical network (i.e. the strength of the grid) affects the amount of available wind power. Point B which is closer to the base node has over three times larger wind power capacity than point A (319 MWp vs. 101 MWp).

An important discovery is the effect of heat conversion and the COP of it. At point A where the heat grid is very weak, conversion offers only maximum of 52 MWp (approx. 50 %) of additional capacity. Point B has radically stronger heat network, and therefore the heat pumps (COP = 3) can increase the wind power capacity from 319 MWp to 589 MWp (85 % more) and direct resistance conversion (COP = 1) to even 1080 MWp (240 % more).

Table 5.1: Wind power capacity and extra heat produced by heat pumps at different connection nodes and with different conversion strategies (HP = heat pumps, conversion), and the respective shares of wind power in electricity and heat consumptions.

Connection node & conversion strategy	Wind capacity (MWp)	Extra heat (MW / GWh)	Share of wind	
			elec (%)	heat (%)
Point A				
• Without conversion	101	–	5.3	–
• HP (COP = 3) at point A	112	33 / 0.24	5.8	0.004
• HP (COP = 3) downstream	145	134 / 17.6	7.4	0.27
• HP (COP = 1) at point A	135	35 / 0.27	7.0	0.037
• HP (COP = 1) downstream	153	53 / 9.6	7.7	0.15
Point B				
• Without conversion	319	–	16.7	–
• HP (COP = 3) at point B	570	773 / 281	27.5	4.3
• HP (COP = 3) downstream	589	831 / 332	28.1	5.0
• HP (COP = 1) at point B	1070	769 / 754	38.5	11.4
• HP (COP = 1) downstream	1080	779 / 770	38.6	11.8
Points B + C				
• Without conversion	319 + 289	–	31.7	–
• HP (COP = 3) at points B, C	570 + 483	1370 / 464	51.3	7.0
• HP (COP = 1) at points B, C	1070 + 873	1367 / 1293	71.6	19.6

By dividing the connection among two separate connection points, the capacity may be lifted to almost 2 GWp.

With resistance conversion, wind power could provide almost 40 % of the total electricity demand in Helsinki if the farm is connected to point B. With the help of point C, the share is over 70 %.

The reason, why resistance conversion allows larger wind capacities than heat pumps, is that the limitations for the conversion at the connection node come from the heat grid. To produce the same (limiting) amount of heat with electric resistance requires three times more electricity than heat pumps. With downstream conversion, the situation is not the same since in that case the limitations are partly due to the electrical network (i.e. how much electricity it is possible to transport for the conversion).

Wind farms of size 600 MWp or even over 1 GWp are huge and no such farm exists in the world at the moment. However, the United Kingdom has that kind of a farm under construction [49].

One significant observation is that the conversion increases the share of wind power also in electricity consumption quite significantly—even though the flow channels are constant and momentarily any higher electricity peaks cannot be imported away from the nodes. The increase happens because the wind production profile is so strongly fluctuating. The higher peaks are still cut off but many there are many smaller peaks that have room to grow before the conversion limit strikes them.

Although the wind shares in heat consumption are small compared to the electricity, they are not totally negligible. 5 % of heat, for example, is already a somewhat significant step in the transition away from the fossil energy, especially as it originates from a win-win situation where heat conversion makes it possible to increase the renewable electricity production at the same time as they produce renewable heat.

Figure 5.4 shows an example how the wind energy is distributed to the city. There are the shares of wind power produced energy in the cases where the maximum amount of wind power is connected to point B, which means 319 MW without heat pumps and 589 MW with them. It shows how the energy flows more downstream than upstream. The case in question is able to provide some wind-produced heat also for the furthest nodes from the wind farm connection (about 3 % of the heat demand of the nodes).

5.3 Solar power and electric vehicles

The other main topic in Helsinki was solar power with electric vehicles. This case does not take the heating network into account. It was assumed that Helsinki wants to add 2 GWp of solar electricity into its energy system. First question was where the solar panels should be

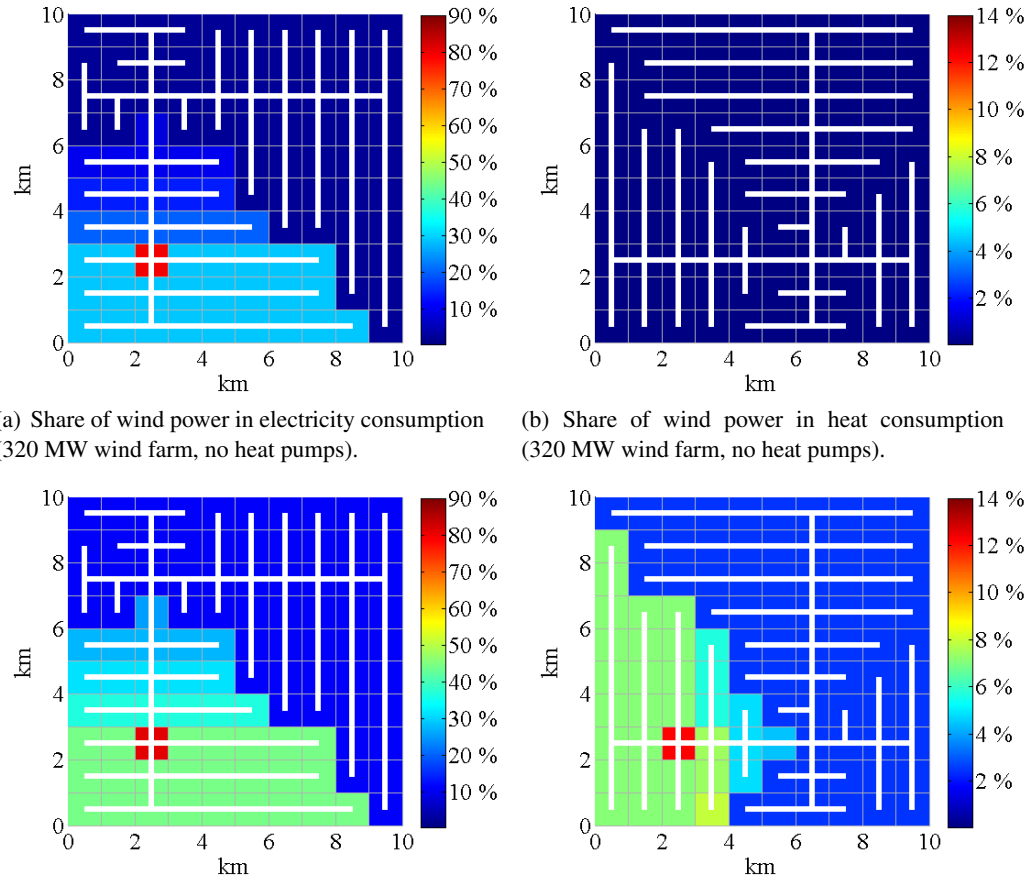

(a) Share of wind power in electricity consumption (320 MW wind farm, no heat pumps).

(b) Share of wind power in heat consumption (320 MW wind farm, no heat pumps).

(c) Share of wind power in electricity consumption (590 MW wind farm, with heat pumps).

(d) Share of wind power in heat consumption (590 MW wind farm, with heat pumps).

Figure 5.4: Share of wind power produced electricity and heat in respective consumptions. The upper figures represent the case of 320 MW with no heat pumps and the lower ones the case of 590 MW with heat pumps.

installed and what kind of overflows the installation causes.

Figure 5.5 shows the three different cases how the PV panels could be allocated among the nodes. The left hand side shows the PV distribution and right hand side the respective overflows that are caused by the PV production. In the uppermost case, the PVs are allocated according to consumption, and in the undermost case, they are equally everywhere. The case in the middle is a linear combination of those two cases.

2 GWp of solar electricity is clearly too much for the electrical network. With equal PV distribution, the city center is not a problem and there are no overflows, but the more distant areas with weaker network lines can suffer overflows of almost 100 %. Consumption based allocation produces overflows that are almost as large everywhere, about 30 %. In this case, the problem on top of the overflows may be that the land use (the share of land area covered

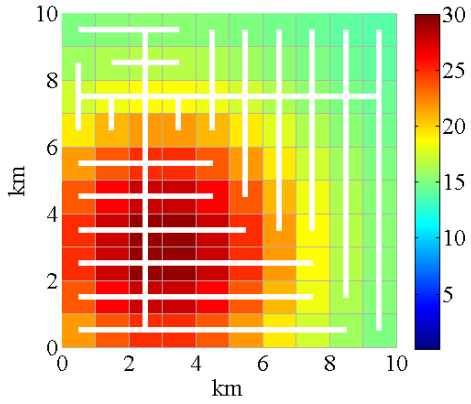

(a) PV distribution in MWp/km^2, consumption based allocation

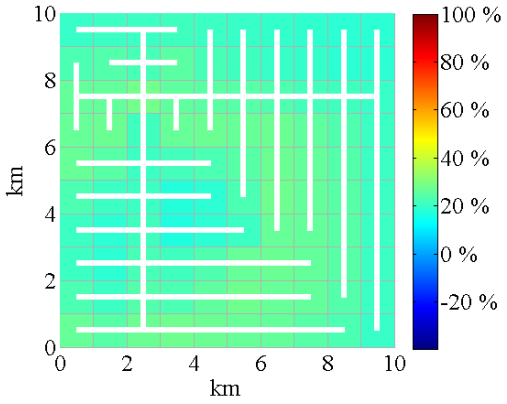

(b) Overflows caused by PVs, consumption based allocation.

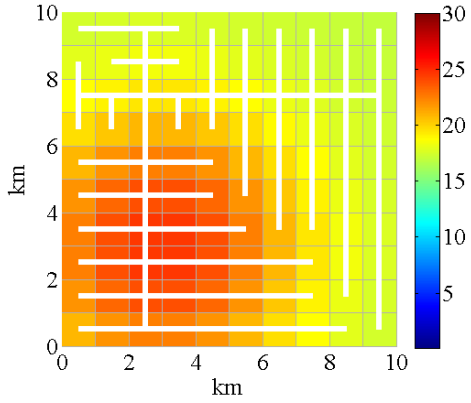

(c) PV distribution in MWp/km^2, half of them allocated according to consumption and half equally everywhere.

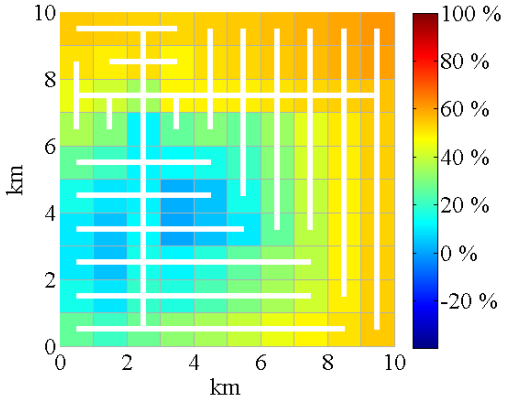

(d) Overflows caused by PVs, half of them allocated according to consumption and half equally everywhere.

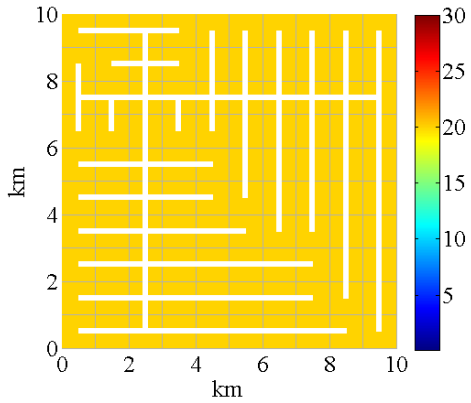

(e) PV distribution in MWp/km^2, equal allocation.

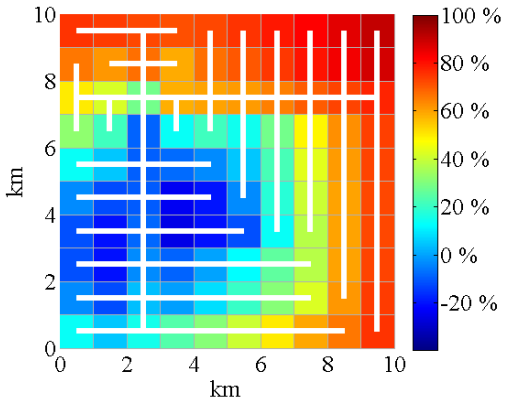

(f) Overflows caused by PVs, equal allocation.

Figure 5.5: PV distributions (left) and the overflows caused by them (right) in three different cases.

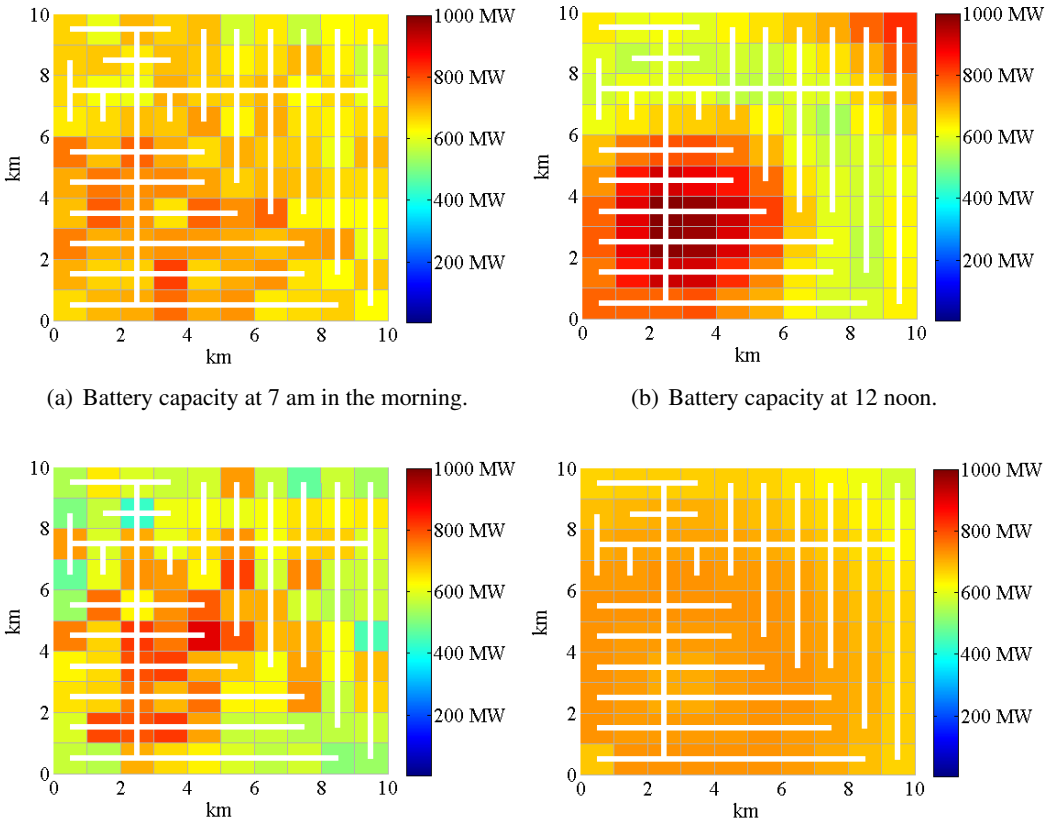

(a) Battery capacity at 7 am in the morning.

(b) Battery capacity at 12 noon.

(c) Battery capacity at 5 pm in the afternoon.

(d) Battery capacity at 11 pm in the evening

Figure 5.6: Battery capacity of 100,000 electric vehicles at four different time steps.

with PV panels) in the city center climbs to about 15 % (with assumption that the cells produce electricity with efficiency of 20 %).

The overflow problem is tried to solve with smart EV charging. Electric vehicles were put to recharge so that the overflows could be reduced (the charging strategy is explained in Section 3.5). The EV simulation was carried out with 50,000 and 100,000 EVs and the time period was limited to one 5-day week at midsummer (June 20 – June 24). The traffic of the cars is represented in Figure 5.6 that shows the battery capacity of the cars. Battery capacity tells directly the spatial distribution of the cars, since it is assumed that each car has a battery of the same size, 10 kWh. The cars concentrate to the city center for the working hours and at nights they are spread more widely throughout the city.

The results how the EV charging may affect the situation, can be seen in Figure 5.7. It shows how the overflows are reduced as the number of cars increases. Already 50,000 cars can significantly ease the overflow stress in the network. The north-east corner drops already to zero (= no overflows) and the areas with worst situation go from 35 % to about

25 %. With 100 000 cars, about half of the nodes undergo no overflows at all or they are very small (under 5 or 10 %). In this simulation, the maximum momentary power of EV charging was 17 MW.

Figure 5.7(c) has a circular area that does not go to zero because of two reasons. First, the starting situation (Figure 5.7(a)) is worse. This however does not explain the whole case, since the overflows drop from 25 % to zero at the city center but on that circular area, the drop is only 10 percentage points or a bit more. The other reason is that the worst overflows happen normally at noon when the sun shines brightly. At that time, the cars are concentrated to the city center (Figure 5.6(b)) and the charging capacity of the circular area is thus much weaker.

The case where the solar cells were allocated equally everywhere was also studied, but the overflow situation in that case was such that even 100,000 cars could not bring any advantage. The maximum overflow peaks stayed as high as they were before the EV charging. The reason for this was that the batteries of the cars were already full during the highest solar production peaks. Increasing the number of the cars or the size of their batteries could be one solution but maybe a better way would be developing smarter charging strategies. The strategy used here did not take the time when the maximum production peaks occur into account. The cars were recharged if there were overflows (even tiny ones) springing up. The case drifted to a situation where the batteries were already full but the highest production peaks were not reached yet. With a charging method that could forecast the moment of the maximum overflow, it would be possible to recharge at the right time and not just naively once even small overflows are born.

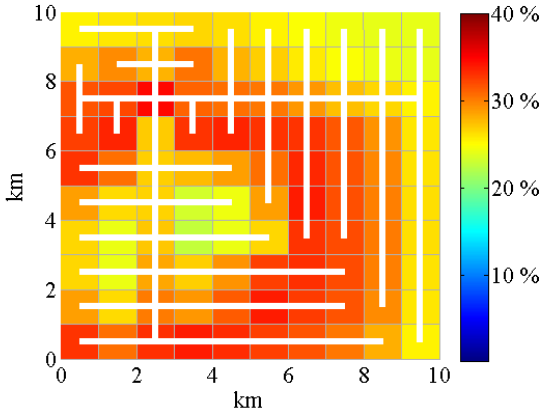

(a) No EVs

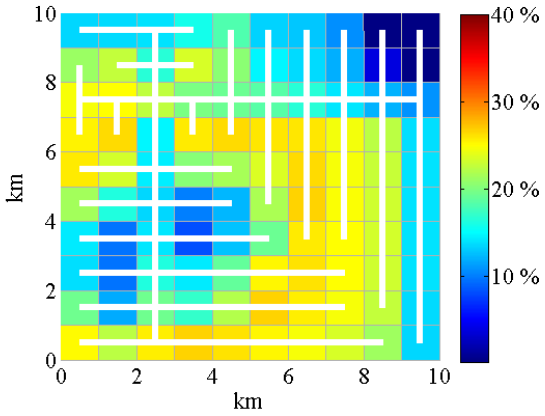

(b) 50,000 EVs

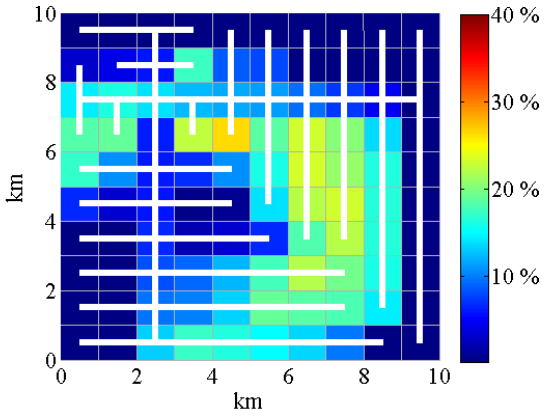

(c) 100,000 EVs

Figure 5.7: Maximum overflows at one midsummer week and the effect of smart EV charging on them. Consumption based PV allocation.

Chapter 6

Shanghai case study

6.1 Reference case

The simulations were started from the reference case, which included conversion from electricity to heat and cooling. The reference case defines the flow channels. Shanghai has two networks that were studied, electricity and gas. The gas network was assumed to be strong enough to transport all the gas needed, and thus the only flow channel limitations come from the electrical grid. The channels are represented in Figure 6.1.

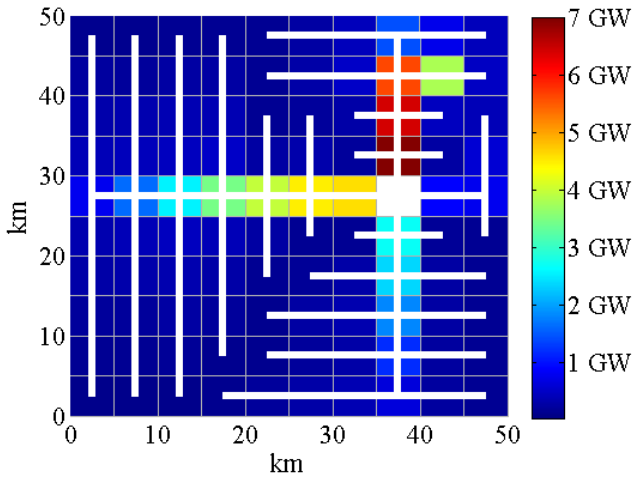

Figure 6.1: Flow channels of Shanghai electrical network. The colour of the node represents the channel of the line pointing towards the white base node. The network is shown by white lines.

6.2 Photovoltaics scheme

The first target was to add so much solar production to Shanghai that momentarily their production equals the consumption of the city. This case is called "PV 100 %". This kind of a self-use limit (no PV-produced electricity exported outside the city) sets the amount of possible solar power installations to 19.3 GWp. How the PV panels are allocated for the nodes, is represented in Figure 6.2(a). 19.3 GWp is a huge amount (about half) compared to the current amount of PV installations in the world (see Figure 2.4). This fact reveals how much capable and unused potential for solar energy there is still in the world.

With 19.3 GWp in Shanghai, 21 % of the electricity consumption (including electricity for heating and cooling) is covered by PV. Because part of the heating (43.7 %) and cooling load (82.0 %) is covered with electricity, some of this energy originates from the solar production. When calculated all electrical, heating and cooling energy demands together, 18 % of this total energy comes from renewable sources. The term *total energy* thus includes all final energy consumption except traffic that is not studied in this thesis.

"PV 100 %" case does not cause any overflows (figure 6.2(b)). This suggests that even more PV power could be installed in the system. Figure 6.3 shows the electricity that is imported from outside to the city (i.e. the electricity that is produced by some other means than PV). At 1020th hour (= at noon on 12th of February) the imported electricity goes to zero which means that all electricity demand is met by photovoltaics. However the graph is very fluctuating (only few high peaks) and if a few peaks would be allowed to exceed the self-use limit, radically more PV power could be installed.

Another case was studied where 1 % of produced PV electricity is exported away from

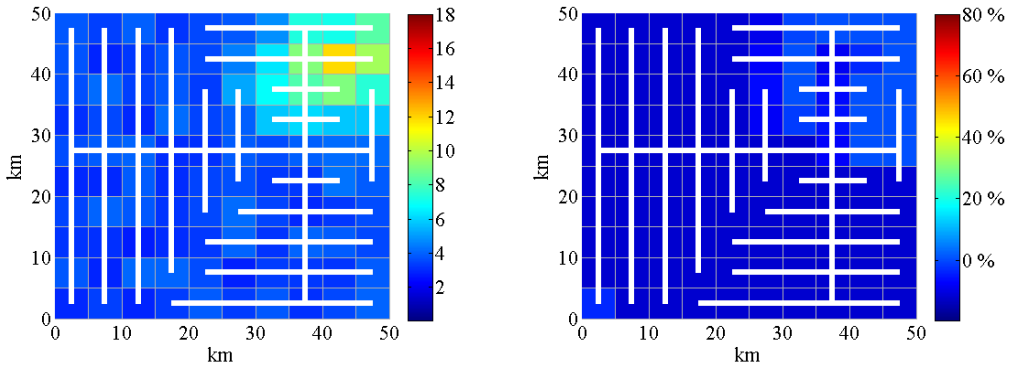

(a) PV distribution in MW/km^2. (b) Maximum overflows caused by PVs.

Figure 6.2: Solar cell distribution and maximum overflows in case "PV 100 %" where 19.3 GWp were installed in Shanghai energy system.

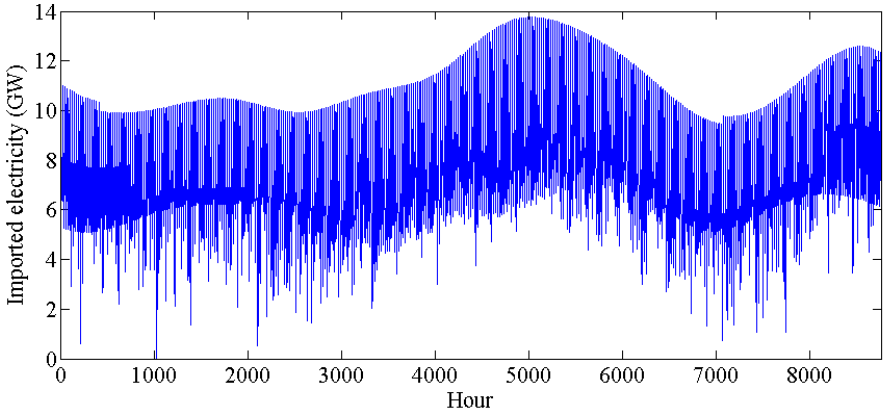

Figure 6.3: Imported electricity (electricity produced by some other means than PV) throughout a year in case "PV 100 %".

the city. In this case, the PV capacity rose to 28.6 GWp which is 148 % of the PV amount in "PV 100 %" case. For this reason this case is called "PV 150 %". This amount of PV panels could cover 31 % of the electricity consumption and 27 % of the total energy consumption of the city. All these numbers are gathered with the trigeneration cases of the next section to Table 6.1 on page 63.

Figures 6.4 and 6.5 depict the case "PV 150 %". Figure 6.5 shows how some peaks exceed the self-use limit and some energy is exported away from the city. Figure 6.4(a) shows that the PV density is almost 18 MWp/km^2 in the city center. This is rather small compared to the highest values studied in Helsinki (Figure 5.5(a)), so the physical space for

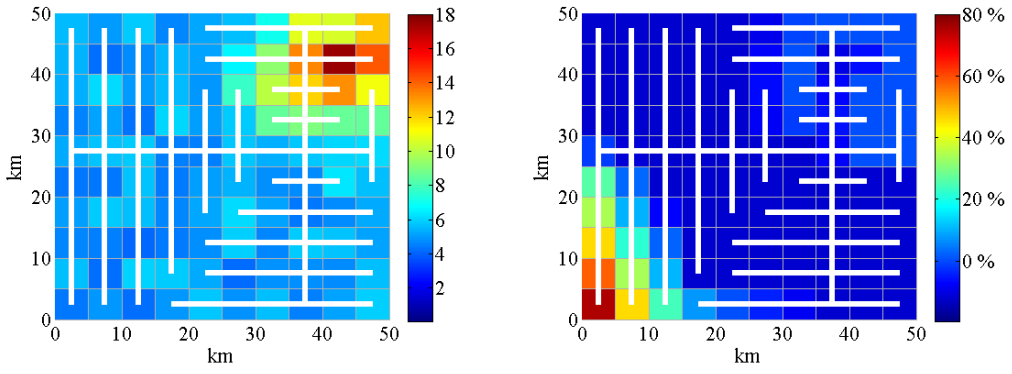

(a) PV distribution in MW/km^2.

(b) Maximum overflows caused by PVs.

Figure 6.4: Solar cell distribution and maximum overflows in case "PV 150 %" where 28.6 GWp were installed in Shanghai energy system.

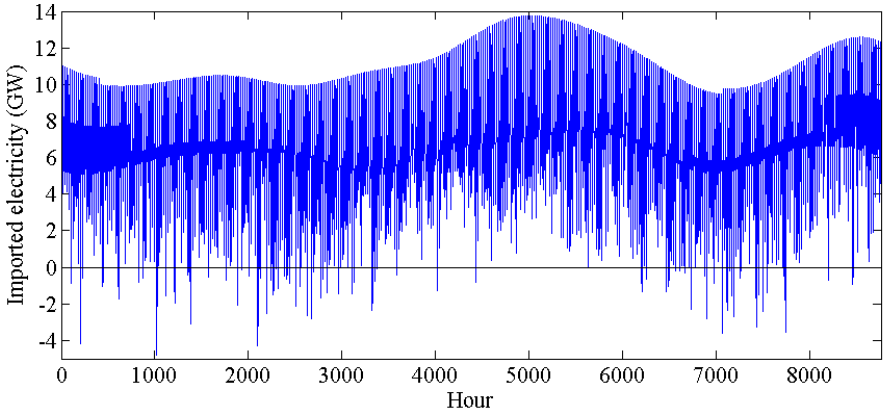

Figure 6.5: Imported electricity (electricity produced by some other means than PV) throughout a year in case "PV 150 %".

the panels should not be a problem. The problem however may be the fact that most distant parts of the city suffer momentarily high overflows (Figure 6.4(b)). The production peaks there are thus too high compared to the consumption.

Figure 6.6 shows in average where the electricity is produced that is consumed at the center node. The average consumption of the center node is about 1800 MW, major part of which comes from outside the grid (1600 MW). Local PV panels produce 85 MW and the rest is transported from other nodes. The most distant nodes provide almost 4 MW each for the center node; where as the neighbouring nodes of the center can achieve only 2 MW.

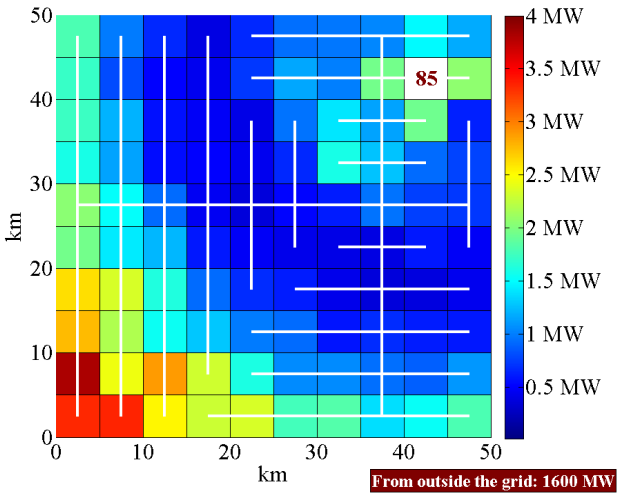

Figure 6.6: Production distribution of electricity which is consumed at the Shanghai center node in case "PV 150 %" (average power throughout a year).

This shows how much there is overproduction in the outskirts.

There is a slight mismatch between Figures 4.15(c) and 6.6 concerning the average center node electricity consumption. Figure 4.15(c) shows that it is 57 MW/km^2 $\times$ 25 km^2 = 1425 MW, which is smaller than 1800 MW mentioned previously in this section. The difference is due to Figure 4.15(c) does not take the electricity that is converted to heat and cooling into account but Figure 6.6 does.

6.3 Trigeneration in city center

The city center has a very high consumption peak and it is not possible to produce there so much solar power that it would satisfy the local demand. The panels require land or roof area which is always limited. Distributed energy production was however wanted there, which why a fuel cell based trigeneration system was installed in the city center. *City center* means here usually the nine nodes in the north-east corner of the city, i.e. the ones around the center point at coordinates 42.5 km, 42.5 km.

6.3.1 Replacement of photovoltaics to avoid overflows

The first case with trigeneration system in the city center is called "PV+trig 150 %" since the starting point was case "PV 150 %". The overflow problems born there were solved by removing some PV panels from the overflow areas and by replacing their production capacity with trigeneration production in the center node (only one node, not the whole center of 9 nodes). The electrical power of the trigeneration system was set to the maximum production of the removed panels. In this case it was 140 MW (which is smaller than the nominal power of the removed cells 263 MWp).

Because a fuel cell with 140 MW electrical output is quite small, it can be operated on full power throughout a year. Heat and electrical efficiencies of the cell are 40 %, and thus the cell produces every hour 140 MW of heat and electricity. Cooling is not done at all, since all thermal energy may be used for heating purposes. This way, the system may be thought to be more traditional cogeneration fuel cell plant without absorption chillers.

Figure 6.7 shows relatively how the production capacity is changed compared to "PV 150 %" case (Figure 6.4. Figure 6.8 reveals that the overflow problem was solved by this kind of a minor relocation of production. The center node has room for large-scale distributed generation due to its high consumption, and thus the added 140 MW had no visible effect.

By replacing fluctuating solar power with constant fuel cell production, the amount of produced energy increases. This can be seen in Table 6.1. Total share of distributed energy has risen about 6 % (from 26.5 % to 28.1 %), and the share of distributed electricity has also

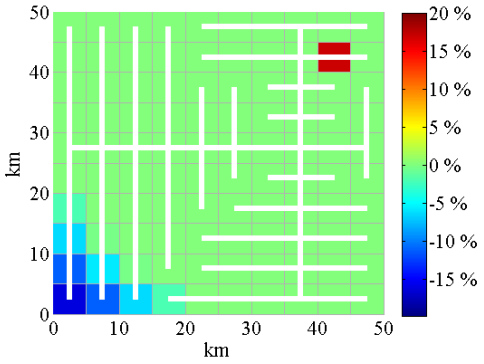

Figure 6.7: Relative change in electricity production capacity between cases "PV 150 %" and "PV+trig 150 %".

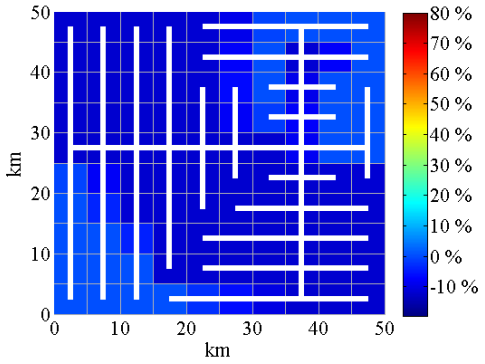

Figure 6.8: Maximum overflows caused by case "PV+trig 150 %".

increased almost 4 % (from 31.1 % to 32.2 %). These numbers are quite large compared to the fact that the solar power production replaced by fuel cells was only about 0.5 % of the whole PV capacity.

6.3.2 Photovoltaics in addition to large scale trigeneration

The trigeneration cases of this section do not break the self-use limit that was considered previously also with PV-only cases in Section 6.2. Figure 6.9 shows how much PV power fits to the energy system without breaking the self-use limit of electricity production if certain percentages of the cooling and heating demand are satisfied with trigeneration. The horizontal axes represent the shares of respective energy consumption that is met with trigeneration at each hour.

The self-use limit of PVs without trigeneration was 19.3 GWp (Section 6.2) which is the highest point of the graph in Figure 6.9. The effect of cooling production on the electricity is much stronger than the one of heating. This is due to two reasons. First, the cooling load is larger than the heating load, and second, one unit of produced cooling energy produces more electricity than the same amount of produced heat. Because the COP when converting heat into cooling is 0.7, one unit of cooling produces about 1.4 ($\approx \frac{1}{0.7}$) units of electricity. Heat and electricity are produced with 1:1 ratio.

The radical drop at around 83 % share of trigeneration heat occurs because at this point the electricity produced with trigeneration exceeds already the self-use limit. This happens on 20th of January at 4 am (460th hour of the year). This is a night time moment, so there is no PV production then. Thus, adding some PV power would not make the situation any worse, but the self-use limit is still broken. It is not possible to define the amount of PV

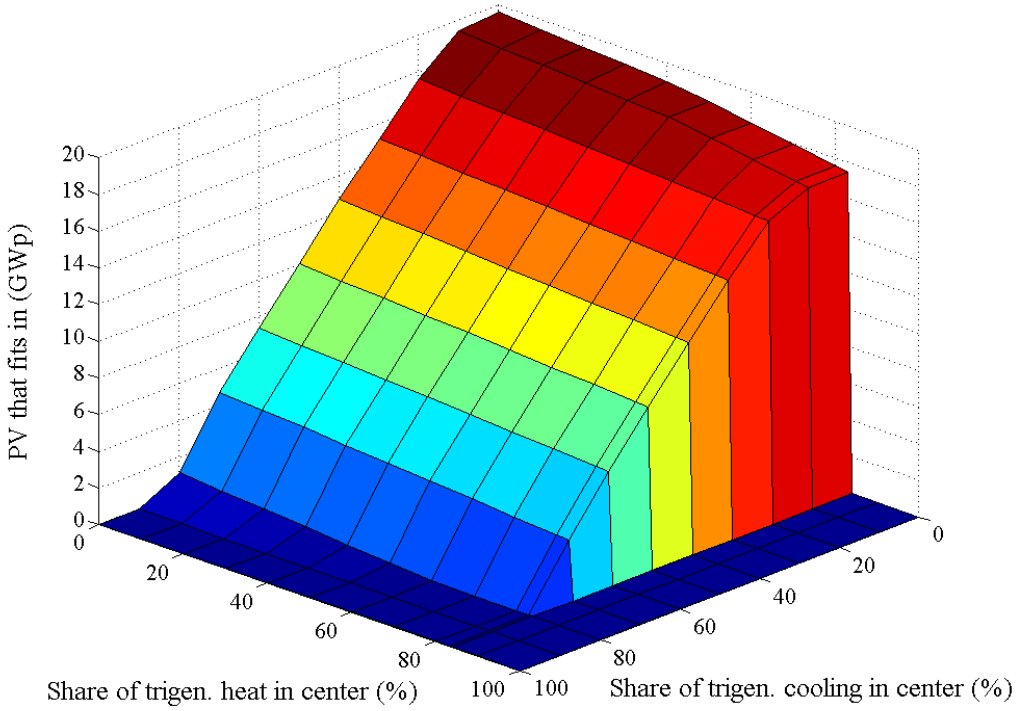

Figure 6.9: The amount of PV production that fits into the energy system without violating the self-use limit of electricity as a function of the shares of trigeneration energy in heating and cooling load in the city center.

that would break the limit already broken. The values however are marked as zeros in the graph.

Two points from the figure were chosen under more thorough inspection. These were the case where 25 % of heating and 25 % of cooling are made with trigeneration, and the case with the corresponding percentages 50 % and 50 %. The cases are called “Trig 25–25” and “Trig 50–50”, respectively. These two cases are represented in Table 6.1 with the PV cases studied previously.

Making 25 % of the thermal energy in the city center with trigeneration systems (case “Trig 25–25”) means that the electricity production capacity of the fuel cells in the city center is 3.7 GW. A fuel cell installation of this size allows 16.0 GWp of PV panels in the city without breaking the self-use limit. If the trigeneration percentage in the center is increased to 50 %, the PV capacity drops to 9.3 GWp. PV capacities of this size are huge when comparing to the current installations in the world (Fig. 2.4).

The greatest advantage of trigeneration systems relates to the shares of distributed energy

in the whole energy consumption. When assuming that the self-use limit is obeyed, the PVs could provide 21 % of the electricity, and about 18 % of the total energy consumption. Both of these numbers could be increased to over 31 % with the fuel cell trigeneration in the center.

Table 6.1: Results of distributed PV and trigeneration cases in Shanghai

Case*	PV (GWp)	PV share of elec (%)	Trigener. elec (GW)	Share of DEGS in elec (%)	Share of DEGS in energy (%)
PV 100 %	19.3	21.0	–	21.0	17.9
PV 150 %	28.6	31.1	–	31.1	26.5
PV+trig 150 %	28.4	30.8	0.14	32.3	28.1
Trig 25–25	16.0	17.8	3.7	27.9	28.4
Trig 50–50	9.3	10.5	7.3	31.1	31.5

*The percentage in three topmost cases refer to self-use limit of electricity and the numbers in two undermost cases are the shares of heating and cooling demands (respectively) satisfied with trigeneration in the city center.

Chapter 7

Summary and conclusions

This work presents a simulation model for smart multiple energy carrier networks. Different energy carriers (electricity, district heating, natural gas, electric vehicles etc.) are modelled interactively to enable large-scale penetration of distributed, renewable and intermittent energy sources into the present energy system. One of the main advantages having interacting energy networks is the possibility to solve bottlenecks occurring in some network through utilizing the other ones. This method also allows to study the energy system as a whole with the emphasis more on the final energy use rather than on energy production only.

In the simulation model the urban area is divided into nodes that represent suburbs, blocks of houses or even single buildings in the city. To each node a consumption and production profile of the energy carriers is attached. Nodes are interconnected by energy networks. The model makes it possible to track spatially the energy flows in the whole city area.

The model presented here proved to describe spatial and temporal energy profiles and their variations of a whole city conveniently. It is a good tool for analyzing interacting energy carriers and the increased flexibility of the energy system they bring along. Despite the several dimensions of the model, the calculation times remained fairly short, in yearly simulations a few minutes at most. One major reason for this was that any iterative calculation methods were avoided, which meant for example that the energy networks have to be loopless.

Another point that kept the model simple is that all energy carriers are measured in same units (MW, MWh). This sets its own limitations to the model, but on the hand, if one wants to know for example the voltage fluctuations of the electric grid, they can be calculated as the energy flows are known. One proof of the functionality of the model was the connection with an external EV simulator.

The program was used to study renewable energy integration in Helsinki and Shanghai. In Helsinki case the question was to find out, how much renewable energy (wind and solar

power) could be installed in the present energy system and how much this share could be increased when employing smart conversion or electric vehicle recharging strategies. In Shanghai the interest was on solar power and local small-scale cogeneration technology.

The results suggest that by enabling electricity-to-heat conversion (electric resistance or heat pumps connected to the district heating system) in Helsinki, it could be possible to increase the capacity of wind power by more than 3-times over a reference system without any conversion. The wind power capacity is strongly dependent on where the wind power is connected to the electrical network and by which technology the electricity-to-heat conversion is done. It was found that the Helsinki energy system could allow through an optimum multi-energy carrier strategy wind power capacity corresponding to even beyond 70 % of all electricity consumption and almost 20 % of the heat on a yearly level.

Another important finding in the Helsinki case was that smart recharging strategies with plug-in electric vehicles could significantly ease the stress that large-scale solar cell installations cause to the electrical network. It was found that 100,000 plug-in hybrids in the city could reduce the overflows created by 2 GWp of solar cells by over 50 %. In several areas, the overflows were cancelled completely, but this requires also smart spatial distribution of PV production. However, the recharging strategies need to be more predictive for optimal timing of the charging capacity.

In the Shanghai case, the energy system could enable solar power up to the so-called self-use limit of electricity. This means that there is a moment in time when all electricity demand of the city could be met by solar power. This would mean a PV capacity of 19.3 GWp. The solar production would cover then about 20 % of the annual electricity demand. If the PV systems were scaled up to 150 % of the self-use limit, the grid would be too weak to transport all produced electricity. However, replacing only 1 % of the PV power capacity with trigeneration in the city center would solve this problem, and the share of distributed electricity production could stand for about 32 % of the annual electricity demand.

Trigeneration proved to be an interesting option for Shanghai city center where the consumption is so high that it would be impossible to find enough space for photovoltaics to cover the demand. Another advantage of the trigeneration is that it increases the distributed heating and cooling energy production. With photovoltaics, trigeneration could lead to a situation where over 30 % of all energy (electricity, heating, cooling) demand were satisfied with these technologies and without exceeding the self-use limit of electricity. With PVs only, the share remained below 18 %.

The model presented here is generic by nature and easily modifiable. Although it fit rather well for its purpose on this work, there are several suggestions for improvements. More powerful tools for optimization and economic analysis could be added as well as

other new energy technologies. The calculation speed and usability of the program could be further enhanced as well.

Several interesting cases were left outside this thesis, for example storage optimization of energy. Different storage technologies will definitely be very important for sustainable energy scenarios and would be worthwhile to investigate. For example, electricity for heating could be stored in thermal energy form also in the cities without the interfacing of district heating. Electricity for cooling purposes could be stored as chilled water.

The role of e-mobility to balance the energy system would also deserve a more detailed analysis. Here, only plug-in-vehicles enabling battery charging was considered. Next step would be to add the option for vehicle-to-grid solutions where electricity would flow in both directions between car battery and grid.

Finally, electricity-to-gas conversion technology may be a future option to consider. For the cities with extensive natural gas network, electrolysis-type of solutions could provide same kind of advantages as electricity-to-heat conversion. Besides, the conversion of gas back to electricity is much easier than that of heat.

Bibliography

[1] A.-M. Borbely and J. F. Kreider, eds., *Distributed Generation – The Power Paradigm for the New Millennium*. CRC Press, 2001.

[2] H. L. Willis and W. G. Scott, *Distributed Power Generation – Planning and Evaluation*. Marcel Dekker, Inc., 2000.

[3] Electricity Advisory Committee EAC, *Smart Grid: Enabler of the New Energy Economy*, Dec. 2008.

[4] J. H. Lienhard IV and J. H. Lienhard V, *A Heat Transfer Textbook*. Cambridge, Massachusetts, USA: Phlogiston Press, 4 ed., 2011.

[5] H. V. Larsen, B. Bøhm, and M. Wigbels, "A comparison of aggregated models for simulation and operational optimisation of district heating networks," *Energy Conversion and Management*, vol. 45, pp. 1119–1139, 2004.

[6] J. Munoz, N. Jimenez-Redondo, J. Perez-Ruiz, and J. Barquin, "Natural gas network modeling for power systems reliability studies," in *Proceedings of 2003 IEEE Bologna PowerTech*, (Bologna, Italy), pp. 1398–1403, June 2003.

[7] M. Geidl, G. Koeppel, P. Favre-Perrod, B. Klöckl, G. Andersson, and K. Fröhlich, "Energy hubs for the future," *IEEE power & energy magazine*, vol. 5, pp. 24–30, 2007.

[8] M. Geidl and G. Andersson, "Optimal power flow of multiple energy carriers," *IEEE Transactions on Power Systems*, vol. 22, pp. 145–155, Feb. 2007.

[9] M. Geidl and G. Andersson, "Optimal coupling of energy infrastructure," in *Proceedings of 2007 IEEE Lausanne Powertech*, (Lausanne, Switzerland), pp. 1398–1403, July 2007.

[10] Z. Chen and F. Blaabjerg, "Wind farm – a power source in future power systems," *Renewable and Sustainable Energy Reviews*, vol. 13, pp. 1288–1300, 2009.

[11] Global Wind Energy Council GWEC, "Wind energy technology." http://www.gwec.net/index.php?id=31.

[12] Renewable Energy Research Laboratory, University of Massachusetts at Amherst, *Wind Power: Capacity Factor, Intermittency, and what happens when the wind doesn't blow?*

[13] H. Holttinen, *The Impact of large scale wind power production on the Nordic electricity system*. PhD thesis, VTT Technical Research Centre of Finland, 2004.

[14] Global Wind Energy Council GWEC, "Wind is a global power source." http://www.gwec.net/index.php?id=13.

[15] European Wind Energy Association EWEA, *Wind in power – 2010 European statistics*, Feb. 2011.

[16] World Wind Energy Association WWEA, *World Wind Energy Report 2010*, Apr. 2011.

[17] European Wind Energy Association EWEA, *Wind Energy – The Facts*, Oct. 2008.

[18] E. O'Grady, "E.ON completes world's largest wind farm in Texas," *Reuters*, Oct. 2009. http://www.reuters.com/article/2009/10/01/wind-texas-idUSN3023624320091001.

[19] Enercon, *E-126/7,5 MW Technische Daten*. http://www.enercon.de/de-de/66.htm.

[20] G. Knier and National Aeronautics and Space Administration NASA, "How do Photovoltaics Work?," Apr. 2011. http://science.nasa.gov/science-news/science-at-nasa/2002/solarcells/.

[21] European Photovoltaic Industry Association EPIA, *Global Market Outlook for Photovoltaics until 2015*, May 2011.

[22] W. Hoffmann, "Towards an effective European industrial policy for photovoltaics." A conference talk in *20th EPIA AGM* in Athens, May 7th–8th, 2004.

[23] M. Peacock, "Solar industry celebrates grid parity," *ABC Sydney*, Sept. 2011. http://www.abc.net.au/news/2011-09-07/solar-industry-celebrates-grid-parity/2875592/?site=sydney.

[24] A. Hawkes, I. Staffell, D. Brett, and N. Brandon, "Fuel cells for micro-combined heat and power generation," *Energy & Environmental Science*, vol. 2, pp. 729–744, July 2009.

[25] U.S. Department of Energy, "Fuel cells – Types of fuel cells," Mar. 2011. http://www1.eere.energy.gov/hydrogenandfuelcells/fuelcells/fc_types.html.

[26] Solar Panels Plus, "Yazaki Solar Air Conditioning Absorption Chiller WFC-S Series 10, 20 and 30 RT Cooling." http://www.solarpanelsplus.com/yazaki-solar-HVAC/.

[27] J.I. San Martín, I. Zamora, J.J. San Martín, V. Aperribay, and P. Eguía, "Trigeneration systems with fuel cells," in *Proceedings of ICREPQ'08*, (Santander, Spain), Mar. 2008.

[28] International Energy Agency, *Transport, Energy and CO2 – Moving Toward Sustainability*, 2009.

[29] U.S. Department of Energy, *QTR – Report on the First Quadrennial Technology Review*, Sept. 2011.

[30] Toyota Europe, "Prius plug-in hybrid." http://www.toyota-europe.com/cars/coming_soon/prius_plugin/index.aspx.

[31] Volvo Auto Suomi, "Volvo esittelee ensimmäisenä uuden sukupolven hybridit," Feb. 2011. http://www.volvocars.com/fi/top/about/news-events/pages/default.aspx?itemid=57.

[32] "The National Travel Survey 2004–2005." A study conducted by the Ministry of Transport and Communications Finland, the Finnish National Road Administration and the Finnish Rail Administration. www.hlt.fi.

[33] R. Niemi and P. D. Lund, "Decentralized electricity system sizing and placement in distribution networks," *Applied Energy*, vol. 87, pp. 1865–1869, June 2010.

[34] J. Mikkola, "Modelling energy flows and balances in parallel networks." Special Assignment in Engineering Physics and Mathematics, Aalto University School of Science, 2011.

[35] R. Meador, *Cogeneration and District Heating: An Energy-Efficiency Partnership*. Ann Arbor Science, 1981.

[36] L. Landau and E. Lifshitz, *Fluid Mechanics*. Oxford, England: Pergamon Books Ltd., 2 ed., 1987.

[37] J. Lindgren, "Energy strategies for electric mobility in urban areas," Master's thesis, Aalto University School of Science, 2012.

[38] City of Helsinki, Environment Centre, "Helsinki environmental statistics." http://www.helsinginymparistotilasto.fi.

[39] Helsingin Energia, *Vuosikertomus 2006 – Yhteiskuntavastuun raportti*, 2007.

[40] Helsingin Energia, "Monta syytä liittyä kaukolämpöön." http://helen.fi/kaukolampo/kl_edut.html.

[41] Fingrid, "Load and generation." http://www.fingrid.fi/portal/in_english/electricity_market/load_and_generation/.

[42] Tan H.W., "Urban Environment and Energy Demand in Shanghai," in *Proceedings of International Workshop on Countermeasures of Urban Heat Islands*, (Japan), Aug. 2006.

[43] J. Yang, *Power System Short-term Forecasting*. PhD thesis, Technische Universität Darmstadt, 2006.

[44] "Daily weather history for Shanghai/Hongqiao." http://www.freemeteo.com.

[45] J. Pfafferott, "Evaluation of earth-to-air heat exchangers with a standardised method to calculate energy efficiency," *Energy and Buildings*, vol. 35, pp. 971–983, Nov. 2003.

[46] Long W.D. and Bai W., "The Impact of Air-Conditioning Use on Shanghai's Energy Situation in 2010." A Report for the China Sustainable Energy Program, Tongji University, Jan. 2006.

[47] Xie D.M., Zhang G.Q., Zhou J. and Zhang Q., "Analysis of building energy efficiency strategies for the hot summer and cold winter zone in China," in *Proceedings of Building Simulation 2007*, (Beijing, China), pp. 1877–1882, International Building Performance Simulation Association, IBPSA, Sept. 2007.

[48] Cogeneration Technologies, "Absorption chillers." http://www.cogeneration.net/Absorption_Chillers.htm.

[49] London Array Ltd. http://www.londonarray.com.